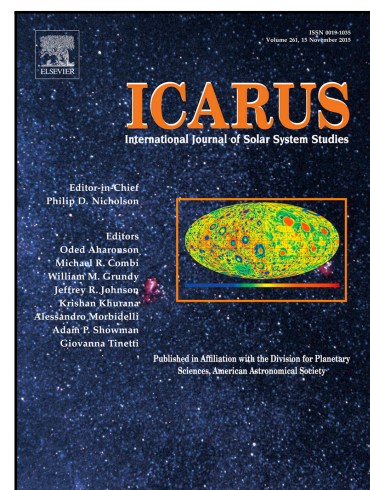


The late accretion and erosion of Vesta's crust recorded by eucrites and diogenites as an astrochemical window into the formation of Jupiter and the early evolution of the Solar System

D. Turrini, V. Svetsov, G. Consolmagno, S. Sirono, M. Jutzi

PII: S0019-1035(17)30438-4
DOI: [10.1016/j.icarus.2018.04.004](https://doi.org/10.1016/j.icarus.2018.04.004)
Reference: YICAR 12860



To appear in: *Icarus*

Received date: 12 June 2017
Revised date: 27 March 2018
Accepted date: 3 April 2018

Please cite this article as: D. Turrini, V. Svetsov, G. Consolmagno, S. Sirono, M. Jutzi, The late accretion and erosion of Vesta's crust recorded by eucrites and diogenites as an astrochemical window into the formation of Jupiter and the early evolution of the Solar System, *Icarus* (2018), doi: [10.1016/j.icarus.2018.04.004](https://doi.org/10.1016/j.icarus.2018.04.004)

This is a PDF file of an unedited manuscript that has been accepted for publication. As a service to our customers we are providing this early version of the manuscript. The manuscript will undergo copyediting, typesetting, and review of the resulting proof before it is published in its final form. Please note that during the production process errors may be discovered which could affect the content, and all legal disclaimers that apply to the journal pertain.

Highlights

- The eucrites and diogenites are differentiated meteorites whose genetic link with the crust of asteroid Vesta was confirmed, together with the survival of said crust, by the NASA mission Dawn
- The composition of some eucrites and diogenites suggests an enrichment in water and highly-siderophile elements in the parent melt of Vesta's crust, interpreted as the record of a late veneer
- The ages of the oldest eucrites and diogenites indicate that Vesta's differentiation occurred early in the history of the Solar System and predates the formation of Jupiter and the other giant planets
- We explore how a late veneer can compositionally and erosionally influence Vesta's crust in a proof-of-concept study focusing on the bombardment triggered by the formation and migration of Jupiter
- The late veneer and the erosion experienced by Vesta's crust during the early collisional history of the asteroid can be jointly used as astrochemical constraints on the early evolution of the Solar System

The late accretion and erosion of Vesta's crust recorded
by eucrites and diogenites as an astrochemical window
into the formation of Jupiter and the early evolution of
the Solar System

D. Turrini^{a,*}, V. Svetsov^b, G. Consolmagno^c, S. Sirono^d, M. Jutzi^e

^a*Institute of Space Astrophysics and Planetology INAF-IAPS, Via del Fosso del
Cavaliere 100, 00133, Rome, Italy.*

^b*Institute for Dynamics of Geospheres, Russian Academy of Sciences, Leninskiy Prospekt
38-1, Moscow 119334, Russia.*

^c*Specola Vaticana, V-00120, Vatican City State.*

^d*Earth and Environmental Sciences, Nagoya University, Tikusa-ku, Furo-cho, Nagoya
464-8601, Japan.*

^e*Physics Institute, Space Research and Planetary Sciences, Center for Space and
Habitability, University of Bern, Sidlerstrasse 5, CH-3012 Bern, Switzerland.*

Abstract

The circumsolar disc was the birthplace of both planetesimals and giant planets, yet the details of their formation histories are as elusive as they are important to understand the origins of the Solar System. For decades the limited thickness of Vesta's basaltic crust, revealed by the link between the asteroid and the howardite-eucrite-diogenite family of meteorites, and its survival to collisional erosion offered an important constraint for the study of these processes. Some results of the Dawn mission, however, cast doubts on our understanding of Vesta's interior composition and of the characteristics of its basaltic crust, weakening this classical constraint. In this work we investigate the late accretion and erosion experienced by Vesta's crust after its differentiation and recorded in the composition of eucrites and diogenites

*Corresponding author.

Email address: diogo.turrini@iaps.inaf.it

April 4, 2018

and show that it offers an astrochemical window into the earliest evolution of the Solar System. In our proof-of-concept case study focusing on the late accretion and erosion of Vesta's crust during the growth and migration of Jupiter, the water enrichment of eucrites appears to be a sensitive function of Jupiter's migration while the enrichment in highly-siderophile elements of diogenites appears to be particularly sensitive to the size-frequency distribution of the planetesimals. The picture depicted by the enrichments created by late accretion in eucrites and diogenites is not qualitatively affected by the uncertainty on the primordial mass of Vesta. Crustal erosion, instead, is more significantly affected by said uncertainty and Vesta's crust survival appears to be mainly useful to study violent collisional scenarios where highly energetic impacts can strip significant amounts of vestan material while limitedly contributing to Vesta's late accretion. While our proof-of-concept case study is based on a simplified physical model and explores only a limited set of scenarios, our results suggest that the astrochemical record of the late accretion and erosion of Vesta's crust provided by eucrites and diogenites can be used as a tool to investigate any process or scenario associated to the evolution of primordial Vesta and of the early Solar System.

Keywords: Asteroid Vesta, Planetary formation, Meteorites, Impact processes, Jupiter

1. Introduction

One of the most challenging tasks in the study of the Solar System is that of disentangling the steps of its formation process that took place during the life of the circumsolar disc, specifically over the timespan extending from the

condensation of the Calcium-Aluminum-rich Inclusions (CAIs) $4568.2^{+0.2}_{-0.4}$ Ma ago, (Bouvier and Wadhwa, 2010) to the dissipation of the gas from the disc 4-5 Myr later (Scott 2006; Johnson et al. 2016; Wang et al. 2017; Kruijer et al. 2017, but values up to 10 Myr are possible based on the comparison with circumstellar discs, see e.g. Fedele et al. 2010). Among the most important events that occurred during this timespan are the formation of the planetesimals, the appearance of the giant planets, and their migration due to their interaction with the nebular gas (see Morbidelli and Raymond 2016 and references therein).

Our understanding of these three processes, however, has been put under scrutiny by new ideas and scenarios. In particular, various authors have argued that the giant planets formed at locations different from their current ones and underwent a period of extensive migration during the life of the circumsolar disk (see Morbidelli and Raymond 2016 and references therein). Such an extensive early migration was shown to be associated with a period of dynamical excitation and orbital remixing of the planetary bodies in the circumsolar disc, with major implications for the evolution of the primordial asteroid belt (Walsh et al., 2011; O'Brien et al., 2014).

However, compositional studies of the asteroid belt (DeMeo and Carry, 2014; Michtchenko et al., 2016) disagree on whether an extensive migration of the giant planets is consistent with the current radial distribution of the different kinds of asteroids. On the other hand, the very mass growth of the giant planets was shown to also be capable of triggering phases of dynamical excitation and radial mixing of the planetesimals even in absence of migration (see Fig. 1 and Turrini et al. 2011, 2012; Turrini 2014; Turrini & Svetsov

2014; Turrini et al. 2015; Raymond & Izidoro 2017). This ambiguity in the early history of the giant planets severely hinders our understanding of the formation of the Solar System.

Most signatures left by these ancient events, like their cratering records, were removed or altered by the later evolution of the individual planetary bodies or of the Solar System as a whole, making it difficult to verify conclusively the different models and scenarios (see Morbidelli and Raymond 2016 and references therein). As our most reliable and temporally resolved source of information on the early life of the Solar System is offered by meteorites, our best chance to solve this conundrum lies in identifying those meteoritic properties that can be linked to the evolution of the nebular environment in which their parent bodies were embedded.

The aim of this work is to investigate how three specific compositional characteristics of the Howardite-Eucrite-Diogenite (HED) family of basaltic achondritic meteorites and of their parent body asteroid (4) Vesta can be jointly used to constrain in a quantitative way the early collisional history of the asteroid and, through that, the dynamical evolution of the circumstellar disc, as first suggested by Turrini (2014) and Turrini & Svetsov (2014). The three compositional characteristics we will focus on are: the survival of Vesta's basaltic crust, the enrichment in water of eucrites, and the enrichment in highly-siderophile elements of diogenites.

In exploring the working of the astrochemical constraints provided by these three compositional characteristics, we will consider a proof-of-concept case study focusing on the collisional evolution of primordial Vesta across Jupiter's mass growth in different migration scenarios for the giant planet

101 (the event also labelled as *Jovian Early Bombardment* or JEB, see Fig. 1
 102 and Turrini et al. 2011, 2012; Turrini 2014; Turrini & Svetsov 2014; Turrini
 103 et al. 2015). This case study has been selected as it allows us to reuse previ-
 104 ous simulations and results to explore the sensitivity of these astrochemical
 105 constraints to a number of physical parameters (namely flux, physical char-
 106 acteristics, size distribution and impact velocity distribution of the impactors
 107 and the mass of the primordial Vesta).

108 The rest of this work is organized as follows. In Sect. 2 we will overview
 109 the current state of our understanding of asteroid (4) Vesta and of the HEDs.
 110 In Sect. 3 we discuss in more details the compositional characteristics of the
 111 HEDs and Vesta we aim to use to constrain the early evolution of the Solar
 112 System. In Sect. 4 we describe the theoretical tools and the simulations used
 113 to in our proof-of-concept case study. Readers interested in the working of
 114 the compositional constraints from Vesta and the HEDs can skip this section
 115 bearing in mind that, due to the exploratory nature of this work, some of
 116 the approximations adopted in the case study will be made for reasons of
 117 convenience (e.g. minimizing the need for additional simulations) and will
 118 not fit equally well all investigated scenarios.

119 The numerical results we will discuss in Sect. 5 should therefore be con-
 120 sidered only as illustrative of the joint working of the three compositional
 121 constraints and the consistency of the investigated scenarios with these com-
 122 positional constraints will need to be reassessed in more details in future
 123 works using more complete physical models. Finally, in Sect. 6 we discuss
 124 the general application of the compositional constraints from Vesta and the
 125 HEDs to other scenarios beyond the simplified ones considered in this work.

2. Vesta and the HEDs: witnesses of the beginning

Asteroid (4) Vesta was identified as the possible source of the Howardite-Eucrite-Diogenite (HED) family of basaltic achondritic meteorites more than 40 years ago (McCord et al., 1970; Consolmagno and Drake, 1977). The NASA mission Dawn, which explored the asteroid between 2011 and 2012 (Russell et al., 2012, 2013), recently provided a strong confirmation to the proposed Vesta-HED genetic link (De Sanctis et al., 2012; Prettyman et al., 2012). Because of this genetic link, the achondritic nature of the HEDs implies that Vesta is a differentiated asteroid that experienced global melting (see e.g. Greenwood et al. 2014; Steenstra et al. 2016).

Members of the HEDs family possess some of the oldest formation ages among the meteoritic samples currently available (see e.g. Scott 2007 and Day et al. 2016 and references therein). These ages date the completion of Vesta's differentiation to no later than 3 Myr after the condensation of CAIs (Bizzarro et al., 2005; Schiller et al., 2011). Based on current estimates, this event occurred immediately before the formation of Jupiter and the other giant planets, which is dated between 3 and 5 Myr after CAIs (Scott, 2006; Johnson et al., 2016; Wang et al., 2017; Kruijer et al., 2017). These data therefore imply that the JEB was most plausibly the first violent collisional event experienced by the partially molten crust of Vesta after the differentiation of the asteroid.

Meteoritic data from the HEDs provide us also indications on the duration of the volcanic resurfacing of Vesta and on the timescale of solidification of its crust after the differentiation process completed (see McSween et al. 2011 for a discussion). Specifically, the basaltic eucrites indicate that the outer

basaltic crust of Vesta formed over several episodes of magmatism through a solid conductive lid (Roszjar et al., 2016) that spanned at least 10 Myr (McSween et al., 2011) and possibly up to 35 Myr (Roszjar et al., 2016). Thermal and geophysical models suggest that the conductive lid was a few km thick (3-5 km, see e.g. Formisano et al. 2013; Tkalcec et al. 2013).

In parallel, diogenites indicate that the underlying lower crust slowly solidified over tens of Myr (see McSween et al. 2011 and references therein). Because of the timing of Jupiter's formation mentioned above (i.e. the first ~ 2 Myr after Vesta's differentiation) and of the duration of the bombardment it triggered (~ 1 Myr, Turrini et al. 2011, 2012), across the JEB both the eucritic and the diogenitic layers were in a partially molten state (see e.g. Formisano et al. 2013; Tkalcec et al. 2013 for the results of thermal and geophysical models and McSween et al. 2011; Greenwood et al. 2014; Steenstra et al. 2016; Roszjar et al. 2016 for the meteoritic evidences).

The most recent compositional models of Vesta combining the information provided by the HEDs (in particular in terms of elemental abundances) and by the Dawn mission (in particular the survival of Vesta's basaltic crust and the size of Vesta's metallic core, as discussed below) with astrochemical constraints have eucrites and diogenites as the main components of the upper and lower layers of Vesta's basaltic crust, whose total thickness should range between 20 and 40 km (Mandler and Elkins-Tanton, 2013; Toplis et al., 2013; Consolmagno et al., 2015). The astrochemical constraints used in these models implicitly assume a chondritic or solar composition (in terms of relative abundances, not absolute ones) for the major rock-forming elements, in particular the abundant lithophiles Si, Mg, Ca and Al (see Consolmagno

et al. 2015 and in particular their Sects. 3.2 , 3.3 and 4.3 for a more detailed discussion of this subject).

As all these elements are expected to condense at temperatures greater than 1500 K in the circumsolar disc (see e.g. Consolmagno et al. 2015), this implicit assumption is expected to hold throughout all but the innermost and hottest region of the circumsolar disc, spanning a fraction of au. According to these compositional models, Vesta's Fe-rich core, which the Dawn mission estimated to possess a radius of 110-140 km (Russell et al., 2012; Ermakov et al., 2014), is overlaid by a mantle composed of harzburgite containing 60-80% olivine (Mandler and Elkins-Tanton, 2013; Toplis et al., 2013; Consolmagno et al., 2015).

Vesta's differentiated nature and the limited thickness of its crust inferred by the Vesta-HED link made the survival of this crust an important constraint for the study of the evolution of the asteroid belt and the Solar System (see Davis et al. 1985; Coradini et al. 2011; O'Brien and Sykes 2011 and references therein, Turrini et al. 2011; Brož et al. 2013; Turrini 2014; Turrini & Svetsov 2014; Consolmagno et al. 2015; Pirani and Turrini 2016). However, some of the very results of the Dawn mission cast doubt on the reliability of the assumption of chondritic bulk composition for the major rock-forming elements of the present-day Vesta (Jutzi et al., 2013; Clenet et al., 2014; Consolmagno et al., 2015; Turrini et al., 2016).

Specifically, the Dawn mission revealed the existence of two giant, partly overlapping impact basins, named Rheasilvia and Veneneia, in the Southern hemisphere of Vesta (Schenk et al., 2012) and confirmed the survival of Vesta's crust at all spatial scales, including inside these two giant basins (De

Sanctis et al., 2012; Ammannito et al., 2013; Ruesch et al., 2014). Simulations of the formation of both impact basins suggested a total excavation depth of 40-80 km (Jutzi et al., 2013) and independent impact and geologic studies (Ivanov and Melosh, 2013; Ruesch et al., 2014) reported an excavation depth of about 30-45 km for the Rheasilvia basin alone, values at odds with the thickness of Vesta's crust reported by the most recent compositional models (Mandler and Elkins-Tanton, 2013; Toplis et al., 2013; Consolmagno et al., 2015).

More precisely, it has been pointed out that the lack of olivine signatures inside the two partly overlapping impact basins Rheasilvia and Veneneia and on Rheasilvia's central peak (Jutzi et al., 2013; Clenet et al., 2014; Ruesch et al., 2014), Vesta's density profile and the mass balance of its interior structure estimated by Dawn (Consolmagno et al., 2015), and the likely exogenous origin of the limited olivine-rich material on Vesta's surface in the Northern hemisphere (Turrini et al., 2016) are all inconsistent with the limited thickness of said crust associated with a chondritic bulk composition in terms of the major rock-forming elements (Consolmagno et al., 2015). This argues for a thicker crust of Vesta, which in turns argues for a non-chondritic bulk composition of the present-day asteroid in terms of its major rock-forming elements (Consolmagno et al., 2015).

Consolmagno et al. (2015) discussed this apparent mismatch between the information provided by the HEDs and that coming from Dawn and proposed a possible solution, postulating that the asteroid formed from chondritic material and, after differentiating but before solidifying completely, underwent some altering event that changed its bulk composition to its present one.

226 One proposed event that could produce the required alteration would be a
 227 grazing collision of a larger primordial Vesta with a body of comparable size
 228 stripping a significant fraction of its mantle while preserving most of its crust
 229 (Consolmagno et al., 2015).

230 Another possibility is that, following the catastrophic disruption of pri-
 231 mordial Vesta, the mantle olivine would be more easily fragmented into
 232 smaller bits which could be preferentially swept away by gas drag, leaving
 233 larger basaltic fragments to reaccumulate onto an intact metallic core (Consol-
 234 magno et al., 2016). Other scenarios might be possible, including the ex-
 235 istence of many HED parents whose material might have been reaccumulated
 236 into the asteroid we today call Vesta (Consolmagno et al., 2015). Nonethe-
 237 less, three common traits to all scenarios discussed to date are that pri-
 238 mordial Vesta should have been more massive than present-day Vesta, that
 239 the altering event is suggested to be linked to impacts, and that the altering
 240 event should have occurred while Vesta was still partially molten or possessed
 241 enough radiogenic heat to eliminate any macroporosity created during the
 242 alteration in order to fit the constraints posed by Dawn (Consolmagno et al.,
 243 2015).

244 In principle, finding those evolution tracks for the early Solar System
 245 that, within this scenario for Vesta's evolution, can produce the required
 246 altering event or collision can offer a substitute for the classical constraint
 247 posed by the survival of Vesta's basaltic crust. However, as the primordial
 248 mass of Vesta is currently unconstrained and different evolution tracks can
 249 produce the required alteration (Consolmagno et al., 2015, 2016), attempting
 250 to study the early evolution of the Solar System using one of these scenarios

alone represents an ill-posed problem. What is required, therefore, is a new and general constraint that does not strongly depends on Vesta's primordial mass and that could be applied to all possible scenarios.

3. Eucrites and diogenites: astrochemical constraints on the late accretion and erosion of Vesta

From the time Vesta differentiated to the moment its crust solidified completely, the eucritic and diogenitic layers were altered by impacts (Turrini et al., 2011, 2012; Day et al., 2012; Turrini, 2014; Turrini & Svetsov, 2014; Sarafian et al., 2014). This alteration manifested in two ways. On one hand, impacts removed material from the vestan crust by ejecting part of the mass excavated during the crater formation process at speeds exceeding the ejection velocity of the asteroid. This mass loss process is also known as *cratering erosion* (Davis et al., 1979). On the other hand, impacts delivered mass to the vestan crust in the form of the material from the impacting bodies that survives the collision. This mass accretion process is known as *late accretion* or, when specifically referring to the alteration of the crust of planetary bodies by impacts, *late veneer* (see e.g. Day et al. 2016). From a geologic point of view, in this work we will specifically focus on the late veneer process.

As discussed in Sect. 2, from the meteoritic data supplied by the HEDs we know that Vesta's basaltic crust formed over several magmatic effusive events through a conductive solid lid (Roszjar et al., 2016) with an estimated thickness of a few km (Formisano et al., 2013; Tkalcic et al., 2013). These effusive events could have been either volcanic (the "heat-pipe" mechanism, Moore et al. 2017) or impact-triggered (Turrini, 2014; Turrini & Svetsov, 2014): the shock wave created by an impact, in fact, damages the surface

material at greater depths than those excavated by the crater itself (Melosh, 1989), therefore creating paths for the magma to reach the surface. During this global effusive resurfacing, the outer layer of Vesta's crust acting as the conductive lid would be in a dynamic equilibrium state, with newer material replacing and pushing downward the older one (Moore et al., 2017) together with any contaminant delivered by impacts.

As a consequence, the late veneer of the basaltic eucritic layer could span an interval of at least 10 Myr (see McSween et al. 2011 and references therein, Roszjar et al. 2016). During this temporal interval, material delivered to Vesta's surface would contaminate the basaltic eucrites either by direct injection into the melt or by later incorporation into the magma (Turrini & Svetsov, 2014). The late veneer of the diogenitic layers should in principle last longer (at least a few tens of Myr, see McSween et al. 2011 and references therein), but in order to reach the diogenitic melt the material delivered by later impacts would need to either penetrate thicker layers of solid crust or be pushed at depth by the reprocessing and sinking of the conductive lid.

After the complete solidification of Vesta's crust, impacts would contaminate only the howarditic layer formed by the brecciation of solid eucritic and diogenitic materials (see e.g. Turrini et al. 2014, 2016 for an in-depth discussion of this process on Vesta). Consequently, the composition of eucrites and diogenites records the early collisional evolution of Vesta when the crust of the differentiated asteroid was still partially molten. Since the collisional history of a planetary body is strongly coupled to the evolution of the surrounding environment, the composition of eucrites and diogenites provides constraints on the evolution of the circumsolar disc and the early

Solar System. As we will show in the following, these constraints do not depend on the specific value of the unknown primordial mass of Vesta (see Sect. 2 and Consolmagno et al. 2015) but only on the assumption that the primordial Vesta was characterized by a chondritic bulk composition of the major rock-forming elements.

3.1. *Eucrites, diogenites and mass loss*

For a primordial Vesta with chondritic bulk composition in terms of the major rock-forming elements, the composition of eucrites and diogenites and, in particular, their abundance in rare earth elements allows one to constraint the fractional thickness of the original vestan crust (see Consolmagno et al. 2015 and references therein). Specifically, based on astrochemical abundances (see e.g. Lodders 2010 and references therein) *the basaltic crust represented 15 – 21% of the primordial mass of the asteroid* (see Consolmagno et al. 2015 and references therein). This result is independent on the primordial mass of Vesta and *depends only on the asteroid possessing chondritic bulk composition in terms of its major rock-forming elements at the time of its differentiation* (Consolmagno et al., 2015).

Even if Dawn confirmed the survival of Vesta’s crust at all spatial scales (De Sanctis et al., 2012; Ammannito et al., 2013; Ruesch et al., 2014), the historical constraint posed by such survival is weak due to our ignorance of the absolute value of the initial thickness of Vesta’s crust (in place of the relative one supplied by astrochemical constraints), of the original mass of the primordial Vesta and, should it have been larger than that of present Vesta, of the amount of crustal material that could have been removed by the altering event together with the excess mantle material (Consolmagno et

al., 2015).

Until these unknown factors are more precisely quantified, it is difficult to pinpoint the amount of crustal material that can be removed by cratering erosion without producing an asteroid inconsistent with the present-day Vesta (Turrini, 2014). As such, in our proof-of-concept case study we will limit ourselves to *discuss how the estimated mass losses caused by cratering erosion compare to this upper bound of 15 – 21% of the primordial mass of Vesta.*

3.2. Eucrites and water accretion

The first piece of the puzzle provided by Vesta's late veneer is supplied by basaltic eucrites. While Vesta is globally a volatile-depleted body (see Consolmagno et al. 2015 and references therein), the discovery of small apatite crystals in some basaltic eucritic meteorites (Sarafian et al., 2013) indicates that small quantities of water were present while the eucritic layer was solidifying. While measurements of the D/H ratio in apatites were interpreted as suggestive of a carbonaceous chondritic origin of Vesta's water (Sarafian et al., 2014; Barrett et al., 2016), the results of Hartogh et al. (2011) on the D/H ratio of comet 103P/Hartley 2 indicate that comets could also be a compatible source (Turrini & Svetsov, 2014). However, an incompatibility with a cometary origin, if confirmed, would allow to reject all scenarios invoking a major role for comets in delivering water to Vesta.

While the uncertainty associated to such estimates is large, recent work (Stephant et al., 2016a,b; Sarafian et al., 2017a,b) attempts to constrain quantitatively the amount of water initially present in the eucritic melt. Sarafian et al. (2017a,b) report an upper bound to the water content of

the eucritic parent melts ranging between 260-1000 $\mu\text{g/g}$, i.e. 0.026-0.1 wt%. Independently, Stephant et al. (2016a,b) suggest that water should have represented less than 0.2 wt.% of the eucritic parent melts. For a primordial Vesta characterized by a chondritic bulk composition, eucrites should represent about 2/3 of the vestan crust and the latter should represent no more than 15-21% of the vestan mass (see Consolmagno et al. 2015 and references therein). The values estimated by Sarafian et al. (2017a,b) and Stephant et al. (2016a,b) therefore translate in an *upper bound to the water accreted by primordial Vesta of $1-3 \times 10^{-4}$ the mass of the asteroid*, which we will adopt as our constraint on the maximum amount of water that could be delivered by Vesta's late veneer.

3.3. Diogenites and mass accretion

The second piece of the puzzle provided by Vesta's late veneer is supplied by diogenites. Specifically, some diogenites show an over-abundance in highly-siderophile elements (HSEs) with respect to what would be expected following their preferential migration to the vestan core during differentiation (Day et al., 2012; Dale et al., 2012). While this over-abundance in principle could be explained in different ways (e.g. as the result of variations in the local concentration in the vestan magma, see Day et al. 2016 and references therein), the fact that over-abundances in HSEs are often paired with chondritic elemental ratios of these elements suggests that they result from a late accretion or late veneer of chondritic material (see Day et al. 2016 and references therein). A similar pattern was shown to hold also for the most HSE-enriched eucrites, while eucrites containing low abundances of HSEs presented markedly non-chondritic elemental ratios for these elements (see

Day et al. 2016 and references therein, Dhaliwal et al. 2016).

Assuming a chondritic bulk composition for Vesta at the time of this late veneer or accretion, Day et al. (2012) associated the measured enrichment to a total accreted chondritic mass of about 1 – 2% the primordial mass of the asteroid. Because of the uncertainties in this kind of computations and on the amount of chondritic material delivered to the mantle instead of the crust (late accretion vs. late veneer), and because the temporal interval considered in this work (the duration of the bulk of the bombardment triggered by Jupiter’s mass growth is ~ 1 Myr, see Turrini et al. 2011, 2012) is much shorter than the timespan over which diogenites can be altered (at least 10 Myr or more, see above and McSween et al. 2011), we will adopt the range of values estimated by Day et al. (2012) as an *upper bound to the total accreted chondritic mass delivered to Vesta by the late veneer, which should therefore not exceed 1-2% the mass of the asteroid*, keeping in mind that because of said uncertainties the real upper limit could be much lower.

4. Modelling Jupiter’s formation and Vesta’s collisional evolution

In this section we provide a synthetic description of the previous results and of the methods and approximations we used in our proof-of-concept case study to model the collisional evolution of Vesta during the formation and migration of Jupiter, its effects on the eucritic and diogenitic crust and their dependence on different factors. As mentioned in Sect. 1, due to the exploratory nature of this work for reasons of convenience we build on the simulations, methods and results of previous studies. As a result, readers should keep in mind that not all the approximations made will adapt equally

well to the different cases explored and the numerical results should be considered only as illustrative.

For more details on the methods and the dynamical simulations used for the computation of the impact probabilities and velocities we refer the readers to Turrini et al. (2011), for a more detailed discussion of the collisional model we refer the readers to Turrini (2014) and Turrini & Svetsov (2014), while for more details on the numerical model used in the impact simulations we refer the readers to Turrini & Svetsov (2014) and Turrini et al. (2016). Readers interested in a more detailed discussion of the dynamical characterization of the asteroidal impactors on Vesta across the formation and migration of Jupiter are referred to Turrini et al. (2011) and Turrini (2014), while those interested in the dynamical characterization of the cometary impactors are referred to Turrini et al. (2011) and Turrini & Svetsov (2014).

4.1. *Modelling Jupiter's mass growth and migration*

In this study we used the n-body simulations performed by Turrini et al. (2011) and the associated estimates of the impact probabilities on Vesta as the base for our assessment of the erosional and accretional history of primordial Vesta across Jupiter's formation and migration. Those simulations considered a template of the early Solar System composed of the Sun, the forming Jupiter, Vesta and a disk of planetesimals modelled as massless particles, whose dynamical evolution was followed for 2×10^6 years. From a physical point of view, the starting time of this temporal window should be located between 2 and 4 Myr after the condensation of CAIs to allow for Jupiter to complete its formation between 3 and 5 Myr after CAIs.

During the first $\tau_c = 10^6$ years of this simulated timespan, Jupiter's core

would grow from its initial mass $M_0 = 0.1 M_\oplus$ to the critical mass $M_c = 15 M_\oplus$ as:

$$M_{\text{J}_+} = M_0 + \left(\frac{e}{e-1} \right) (M_c - M_0) \times (1 - e^{-t/\tau_c}) \quad (1)$$

where τ_c can be interpreted as the oligarchic growth timescale of Jupiter's core (see e.g. D'Angelo, Durisen & Lissauer 2011 and references therein).

When Jupiter's core reached the critical mass value M_c , the nebular gas surrounding Jupiter was assumed to rapidly accrete on the planet, whose mass would grow as:

$$M_{\text{J}_+} = M_c + (M_J - M_c) \times (1 - e^{-(t-\tau_c)/\tau_g}) \quad (2)$$

where $M_J = 317.83 M_\oplus$ is the final and present mass of Jupiter. The e-folding time $\tau_g = 5 \times 10^3$ years adopted by Turrini et al. (2011) was derived from the hydrodynamical simulations described in Lissauer et al. (2009) and Coradini, Magni, & Turrini (2010).

In their simulations, Turrini et al. (2011) considered four different migration scenarios: 0 AU (no migration), 0.25 au, 0.5 au and 1 au (see Fig. 1). In their simulations Jupiter always started on circular and planar orbits and, in those scenarios where migration was included, started migrating inward as soon its core reached the critical mass of $15 M_\oplus$. This approximation is equivalent to neglecting the distinction between Type I and Type II migration and starting the migration of the accreting planet as soon the characteristic migration timescale of the forming Jupiter became of the order of 10^6 years (see D'Angelo, Durisen & Lissauer 2011 and references therein).

Given that the effects on the asteroid belt of the dynamical excitation of the planetesimals triggered by the mass growth of the forming Jupiter are

negligible before the gas accretion phase (see Turrini et al. 2011 and Raymond & Izidoro 2017), from a physical point of view this approximation can be treated as assuming that Jupiter’s core started forming farther away and migrated to its initial position due to Type I migration before the beginning of the simulations. Moreover, because of the negligible effects of the forming Jupiter on Vesta before the gas accretion phase, to first order the adopted approximated treatment of Jupiter’s mass growth is not in contrast with the shorter timescales and outer formation regions predicted by the so called “pebble accretion” scenario (Bitsch et al., 2015).

After the giant planet begins to migrate, Jupiter’s orbital radius would evolve as:

$$R_{\text{J}} = R_0 + (R_J - R_0) \times (1 - e^{-(t-\tau_c)/\tau_r}) \quad (3)$$

where R_0 is Jupiter’s orbital radius at the beginning of the simulation, R_J is the final orbital radius and $\tau_r = 5 \times 10^3$ years. The simulations performed by Turrini et al. (2011) using a slower migration ($\tau_r = 2.5 \times 10^4$ years) indicate that the flux of impactors on Vesta is not significantly affected by the migration rate.

4.2. Modelling the primordial Vesta

In the simulations of Turrini et al. (2011), Vesta was initially placed on a circular, planar orbit with semimajor axis $a_v = 2.362$ AU. The asteroid was characterized using the best pre-Dawn estimates of its mass ($m_v = 2.70 \times 10^{23}$ g, Michalak 2000) and mean radius ($r_v = 258$ km, Thomas et al. 1997), whose values differ by 2 – 4% from the ones later estimated by the Dawn mission (2.59×10^{23} g and 262.7 km respectively, Russell et al. 2012).

While these values were reasonable before the arrival of Dawn, the results of Consolmagno et al. (2015) suggest that primordial Vesta could have been more massive (see Sect. 1). Because of this uncertainty on primordial Vesta's mass and because a precise assessment of the latter is beyond the scope of this work, we maintained the template of primordial Vesta used by Turrini et al. (2011) and took advantage of the link between impact probabilities and diameter of the asteroid to rescale the impact fluxes to a more massive primordial Vesta's and explore how the three compositional constraints offered by Vesta and the HEDs responded to this change.

We therefore initially considered a primordial Vesta characterized by a diameter similar to its current mean one. This allows us to take advantage of the fluxes of impactors on the asteroid estimated by Turrini et al. (2011) (see Sect. 4.4). Similarly, in simulating the outcomes of impacts at different impact velocities on Vesta, we characterized the target body with the current diameter and surface gravity of Vesta (see Sect. 4.4). This choice allows us to take advantage of the simulations of rocky impactors on Vesta performed by Turrini et al. (2016) and to simulate only the effects of more realistic cometary impactors than those originally considered by Turrini & Svetsov (2014) (see Sect. 4.4).

The probabilistic method used by Turrini et al. (2011) to estimate impact fluxes on Vesta links impact probabilities to Vesta's diameter. As long as Vesta's mass is not so large that the gravity of the asteroid significantly enhances its effective cross-section (see Turrini et al. 2011 and references therein), impact fluxes will scale with the diameter of the asteroid. For the impact velocities estimated by Turrini et al. (2011), this condition is

495 satisfied for a primordial Vesta no more massive than a few times the present
 496 asteroid. Similarly, both the mass erosion (Holsapple and Housen, 2007) and
 497 the mass accretion (Svetsov, 2011) efficiencies scale with the surface gravity
 498 of the target asteroid, which for a given average density will scale with its
 499 diameter.

500 This approach allowed us to estimate, to first order, the mass loss and
 501 mass accretion experienced by primordial Vesta for different values of its
 502 original mass without the need of performing a large number of additional
 503 simulations. More details on the parameters describing Vesta in our colli-
 504 sional simulations are provided in Sect. 4.4, while a discussion of the effects
 505 of a larger mass of the primordial Vesta on our results is presented in Sect.
 506 5 and 6.

507 *4.3. Modelling the planetesimal disk*

508 The planetesimal disk was modelled by Turrini et al. (2011) as a disk
 509 of massless particles evolving under the gravitational influence of the Sun,
 510 Jupiter and Vesta. The disk of massless particles was composed by 8×10^4
 511 particles and extended from 2 au to 10 au. The massless particles initially
 512 possessed eccentricity and inclination (in radians) values comprised between
 513 0 and 3×10^{-2} (Turrini et al., 2011) and were used as dynamical tracers of
 514 the evolution of the planetesimal disk, each particle representing a swarm of
 515 real planetesimals.

516 The number of real planetesimals populating each swarm and their char-
 517 acteristic diameter depend on the adopted size-frequency distribution (SFD)
 518 for the planetesimal disk. In this work we considered a total of four SFDs:
 519 two for primordial planetesimals and two for collisionally evolved planetes-

imals. Each pair of SFDs (primordial and collisionally evolved) refers to a specific nebular environment, namely quiescent or turbulent circumsolar disc.

The massless particles were associated to their diameters by means of Monte Carlo methods. Since this procedure was performed while processing the output of the simulations, the latter did not include the effects of gas drag as they are size-dependent. The choice of neglecting the effects of gas drag allowed us to explore the effects of different SFDs on Vesta's crustal late accretion and erosion without the need to perform a large number of computationally expensive n-body simulations.

While computationally convenient, however, this choice is not dynamically accurate, particularly for km-sized planetesimals, as gas drag acts to damp orbital eccentricities and inclinations, diminishing the population of dynamically excited planetesimals. At the same time, the radial drift caused by gas drag brings more planetesimals into the orbital resonances with Jupiter, which appear to play the leading role in producing the population of impactors on Vesta (see Turrini et al. 2011 and Sect. 5). The results of analogous simulations performed by Weidenschilling, Davis & Marzari (2001), Grazier et al. (2014) and Raymond & Izidoro (2017) indicate that neglecting the effects of gas drag should not alter the results of this study in a qualitative way by cancelling the JEB.

Differently from the previous studies of Turrini (2014) and Turrini & Svetsov (2014), all four considered SFDs were associated to a circumsolar disc possessing a dust-to-gas ratio $\xi_i = 0.005$ inside the water ice condensation line and $\xi_i = 0.01$ outside (see below for details on the density profiles of the individual discs). The water ice condensation line was assumed at 4 au.

545 The mass of solids comprised between 2 and 3 au amounted to about $2 M_{\oplus}$ for
 546 all four SFDs, consistent with the planetesimals having formed within a Min-
 547 imum Mass Solar Nebula (see also Morbidelli et al. 2009 and Weidenschilling
 548 2011).

549 All planetesimals inside 4 au were assumed to be rocky asteroids with an
 550 average density of 2.4 g/cm^3 (chosen as a compromise between the densities
 551 of volatile-poor and volatile-rich asteroids, see Britt et al. 2002; Carry 2012;
 552 Turrini et al. 2014 and references therein) while those beyond were assumed
 553 to be ice-rich cometary bodies, constituted at 50% of their mass by water
 554 ice and at 50% by rock, with an average density of 1 g/cm^3 . Planetesimals
 555 formed between 3 and 4 au were assumed to possess 10% of their mass as
 556 water in the form of hydrated minerals, similarly to carbonaceous chondrites
 557 (Jarosewich, 1990; Robert, 2003).

558 The transition at 3 au, while somewhat arbitrary, is consistent with the
 559 current distribution of low albedo volatile-rich asteroids being the result of
 560 their inward radial diffusion over the life of the Solar System (Michtchenko et
 561 al., 2016). Moreover, the flux of impactors on Vesta originating from beyond
 562 3 au is due to the 2:1 resonance with Jupiter (located at 3.3 au or outward
 563 depending on the Jovian migration, see Fig. 1 and Turrini et al. 2011), so
 564 our analysis is not particularly sensitive to the actual heliocentric distance
 565 of this transition.

566 The four SFDs we considered in our case study are described in more
 567 detail in the following. A comparison of the average diameters of the plan-
 568 etesimals as a function of their orbital distance from the Sun for the two
 569 primordial SFDs is shown in Fig. 2, while in Fig. 3 we show the com-

570 parison between the two collisionally evolved SFDs in the reference orbital
 571 region comprised between 1 and 4 au considered by Weidenschilling (2011)
 572 and Morbidelli et al. (2009) (see Sects. 4.3.3 and 4.3.4 for the discussion of
 573 their extension to the orbital region between 4 and 10 au).

574 4.3.1. *Primordial planetesimals formed in a quiescent circumsolar disc*

575 The first SFD considered was that of a disk of *primordial planetesimals*
 576 formed by gravitational instability of the dust in the mid-plane of a *quiescent*
 577 *circumsolar disc* (Safronov, 1969; Goldreich and Ward, 1973; Weidenschilling,
 578 1980; Coradini et al., 1981). Following Coradini et al. (1981), the circumsolar
 579 disc was assumed to have a density profile $\sigma = \sigma_0 \left(\frac{r}{1\text{AU}}\right)^{-n_s}$, with $\sigma_0 = 2700$
 580 g cm^{-2} being the gas surface density at 1 AU and $n_s = 1.5$. For this SFD,
 581 which we derived from the results of Coradini et al. (1981), the diameters
 582 of the planetesimals that could impact Vesta roughly range between 1 and
 583 40 km, with the bulk of the impactors being constituted by planetesimals
 584 with diameters of 10-20 km (Turrini, 2014; Turrini & Svetsov, 2014). For
 585 more details on the SFD and the associated Monte Carlo method we refer
 586 interested readers to Turrini (2014) and Turrini & Svetsov (2014).

587 4.3.2. *Primordial planetesimals formed in a turbulent circumsolar disc*

588 The second SFD considered was that of *primordial planetesimals* formed
 589 by concentration of dust particles in low vorticity regions in a *turbulent cir-*
 590 *cumstellar disc* (Cuzzi et al., 2008, 2010). Following Chambers (2010), the
 591 circumstellar disc was assumed to possess a density profile $\sigma = \sigma'_0 \left(\frac{r}{1\text{AU}}\right)^{-n'_s}$,
 592 with $\sigma'_0 = 3500 \text{ g cm}^{-2}$ being the gas surface density at 1 AU and $n'_s = 1$
 593 (see Fig. 14, gray dot-dashed line, Chambers 2010). For this SFD, which we

594 derived from the results of Chambers (2010), the diameters of the planetes-
 595 imals that could impact Vesta roughly range between 20 and 250 km, with
 596 the bulk of the impactors being constituted by planetesimals with diameters
 597 of 100-200 km (Turrini, 2014; Turrini & Svetsov, 2014). For more details on
 598 the SFD and the associated Monte Carlo method we refer interested readers
 599 to Turrini (2014) and Turrini & Svetsov (2014).

600 4.3.3. *Collisionally-evolved planetesimals formed in a quiescent circumstellar* 601 *disc*

602 The third SFD we considered was associated to *collisionally-evolved plan-*
 603 *etesimals* formed in a *quiescent circumstellar disc* and was derived from the
 604 results of Weidenschilling (2011). In this study we focused on the SFD of the
 605 asteroid belt that Weidenschilling (2011) referred to as the “standard case”,
 606 i.e. the one produced from a disk initially populated by planetesimals with
 607 a diameter of 100 m (see Fig. 8, Weidenschilling 2011).

608 The resulting population of planetesimals is dominated *in number* by
 609 collisional fragments with km- or sub-km-sized diameters and *in mass* by
 610 a few large planetesimals and planetary embryos. In our estimates of the
 611 collisional evolution of Vesta we adopted as our lower-end cut-off of the SFD
 612 the diameter of 1 km, a choice motivated by the fact that the slope of the
 613 SFD causes sub-km planetesimals to cumulatively supply only a fraction of
 614 the mass contained in km-sized planetesimals (Weidenschilling, 2011).

615 Because of this cut-off, the bulk of the planetesimals impacting Vesta is
 616 in the form of planetesimals with diameters of 1-2 km (Turrini, 2014; Turrini
 617 & Svetsov, 2014). Lowering our cut-off to 100 m would increase the mass
 618 flux on Vesta only by about 10% with respect to that provided by km-sized

619 asteroids.

620 Strictly speaking, the results of Weidenschilling (2011) apply only to the
 621 inner Solar System (i.e. $1 - 4$ au), so in principle they cannot be applied
 622 to the outer part of the planetesimal disk (i.e. $4 - 10$ au) considered by
 623 Turrini et al. (2011). However, the results of Weidenschilling (2008, 2011)
 624 suggest that the collisionally-evolved SFD of the planetesimals in our regions
 625 of interest does not strongly depend on the radial distance.

626 We followed the approach used in Turrini & Svetsov (2014) and adopted a
 627 similar SFD for the planetesimals beyond 4 au, scaling it in mass by the ratio
 628 between the solid mass comprised between 4 and 10 au and that comprised
 629 between 1 and 4 au. For more details on the SFD and the associated Monte
 630 Carlo method we refer interested readers to Turrini (2014) and Turrini &
 631 Svetsov (2014).

632 4.3.4. *Collisionally-evolved planetesimals formed in a turbulent circumstellar* 633 *disc*

634 The fourth and final SFDs we considered was associated to the case of
 635 *collisionally-evolved planetesimals* formed in *turbulent circumstellar disc* and
 636 was derived from the results of Morbidelli et al. (2009). Morbidelli et al.
 637 (2009) found that the best match with the present-day SFD of the asteroid
 638 belt is obtained for planetesimal sizes initially spanning $100 - 1000$ km (see
 639 Fig. 8, Morbidelli et al. 2009), a range consistent with their formation in a
 640 turbulent nebula.

641 The SFD associated to the best-fit case of Morbidelli et al. (2009) shares
 642 most of the characteristics of the analogous one derived by Weidenschilling
 643 (2011), but shows a larger abundance of planetesimals with diameter com-

644 prised between 5 and 20 km (see Fig. 8a, black solid line, Morbidelli et al.
 645 2009) than the SFD by Weidenschilling (2011), which is significantly flatter
 646 in this size range.

647 While the SFD physically extends down to sub-km sizes, we focused our
 648 attention on the effects of this overabundance and maintained the lower-end
 649 cut-off of the SFD at 5 km in diameter also adopted in Morbidelli et al.
 650 (2009). Because of this, the bulk of the planetesimals impacting Vesta is in
 651 the form of planetesimals with diameters of 5-10 km (Turrini, 2014; Turrini
 652 & Svetsov, 2014).

653 As in the case of the SFD by Weidenschilling (2011) discussed in Sect.
 654 4.3.3, we extended the SFD of Morbidelli et al. (2009) beyond 4 au by scaling
 655 the number of planetesimals by a factor equal to the mass ratio of the solid
 656 material contained between 4 and 10 au to that of the one contained between
 657 1 and 4 au. For more details on the SFD and the associated Monte Carlo
 658 method we refer interested readers to Turrini (2014) and Turrini & Svetsov
 659 (2014).

660 4.4. *Modelling Vesta's collisional history*

661 Turrini et al. (2011) estimated the impact probabilities and the associated
 662 impact velocities between the massless particles and Vesta using a statistical
 663 approach based on solving the ray-torus intersection problem between the
 664 instantaneous orbital torus of Vesta and the linearized path of the massless
 665 particle¹ across the time step when the particle crosses Vesta's orbital region

¹Note that the path of the massless particle is linearized only for the computation of its impact probability with Vesta, not for that of the dynamical evolution of the particle.

(see Turrini et al. 2011 for more details on the method). This method is conceptually similar to the analytical method of Öpik (1976) but requires only to average over the mean anomaly of the target body's orbit instead of averaging on anomaly, longitude of nodes and argument of pericenter of both target and impacting bodies.

In evaluating the collisional history of Vesta we focused on the massless particles impacting Vesta from the moment Jupiter's core started accreting its gaseous envelope (i.e. the second 1 Myr in the simulations by Turrini et al. 2011, see the highlighted area in Fig. 4). This conservative choice is motivated by the need to correct for the fact that the early flux of impactors on Vesta in the simulations is dominated by the impacts of those rocky planetesimals orbiting nearby the asteroid that should have been removed during Vesta's formation.

Fig. 5 shows an example of the distributions of impact probabilities and impact velocities for both asteroidal and cometary impactors recorded in the simulations by Turrini et al. (2011) in the scenarios of no migration and 1 au migration of Jupiter. Note that the impact probabilities reported in Fig. 5 refer to the individual impact events recorded in the simulations and are not impact probabilities averaged over the whole populations of impactors as in classical collisional algorithms (see e.g. O'Brien and Sykes 2011 and references therein). Figs. 6 and 7 show respectively the distributions normalized over the impact probabilities of the asteroidal and cometary impact velocities in the four migration scenarios considered in this study (see also Turrini et al. 2011, Turrini 2014 and Turrini & Svetsov 2014 for a more detailed discussion of the distribution of the impact velocities and their causes. Interested read-

ers are referred to Turrini et al. (2011) and Turrini et al. (2012) for details on the algorithm.

The impact probabilities provided by the simulations were converted into fluxes of impactors using the SFDs described in Sect. 4.3. Following the procedure described in Turrini (2014) and Turrini & Svetsov (2014), for each SFD we run a set of 10^4 Monte Carlo simulations. In each run a new mass value was extracted for each impact event recorded in Turrini et al. (2011) and, since each massless particle causing an impact event represents a swarm of real planetesimals, we used the SFD and the impact probability of the impact event to estimate the associated flux of impactors. Combining the information provided by the mass and flux of impactors associated to the impact event with its estimated impact velocity, the eroded mass m_e and the accreted mass m_a were computed (see Sect. 4.5 for details on the method).

We averaged over each set of 10^4 Monte Carlo simulations to estimate the total mass loss and accretion experienced by Vesta for each specific SFD and the associated standard deviations. If, after averaging, the total flux of impactors associated to one of the SFDs amounted to less than one real impact, we set the total mass loss and accretion values to zero for that SFD.

4.5. *Modelling the effects of impacts on Vesta*

To estimate the effects of impacts in terms of both mass loss and mass accretion, we took advantage of the results of Benz and Asphaug (1999) (see Sect. 4.5.1 for details) and Turrini et al. (2016) (see Sect. 4.5.2 for details). In parallel, we performed 3D numerical simulations of impacts of projectiles onto Vesta using a modified version (Svetsov, 2011; Turrini & Svetsov, 2014; Svetsov and Shuvalov, 2015) of the numerical hydrodynamic method SOVA

(Shuvalov 1999; SOVA is an acronym for Solid-Vapour-Air, as the code is designed for simulations of multi-material, multi-phase flows) that includes the effects of dry friction (Dienes and Walsh, 1970).

Dry friction depends on a dimensionless coefficient of friction for which we adopted a value of 0.7, typical for rocks and sand (Turrini & Svetsov, 2014; Turrini et al., 2016). The behaviour and properties of target and projectiles were determined, as in Turrini & Svetsov (2014) and Turrini et al. (2016), through the ANEOS equations of state (Thompson and Lauson, 1972) using input data (i.e., about 35 variables describing properties of a given material) from Pierazzo et al. (1997) and Tillotson's equation of state for Vesta's iron core (Tillotson, 1962).

In the simulations performed with SOVA, Vesta was modelled as a three-layered sphere with radius of 260 km, possessing an iron core with a radius of 110 km (Russell et al., 2012, 2013; Ermakov et al., 2014) and a crust made of granite with a thickness of 23 km (Consolmagno et al., 2015), separated by a mantle composed of dunite. The mass of Vesta was set equal to its present value, 2.59×10^{23} g (Russell et al., 2012). While Vesta was in a partially molten state at the time of the Jovian Early Bombardment, the approximation we adopted is justified by the following reasons.

First, thermal and geophysical models and meteoritic data all suggest that Vesta's basaltic crust was formed over a series of magmatic effusive events through a solid conductive lid. Second, previous studies indicate that Vesta's mass loss due to cratering erosion was mainly a surface process (Turrini, 2014; Turrini & Svetsov, 2014), hence mainly affecting this solid conductive lid. Third, mass loss occurs mainly from the central regions of

the crater where the material strength is generally unimportant (Holsapple and Housen, 2007), since the stresses during the impacts exceed the strength of the excavated material acquiring velocities greater than the escape velocity of the asteroid. This approximation, however, is more realistic for impactors not exceeding in size the thickness of Vesta’s conductive lid (i.e. a few km) than for larger impactors.

As in Turrini et al. (2016), the numerical grid consisted of $250 \times 100 \times 225$ cells over azimuth, polar angle and radial distance respectively, and we assumed bilateral symmetry to model only the half-space in the zenith direction. Cell sizes were $1/40$ of the projectile’s diameter around the impact point and increased to the antipodal point and to the radial boundaries located at distances of about 10 vestan radii. In all impact simulations, the impact velocity vector lied in the reference plane that passed through the origin of the coordinates and was orthogonal to the zenith.

All simulated impacts were assumed to occur at the average impact angle of 45° (Melosh, 1989), while impact velocities varied between 1 and 12 km/s based on the results of the simulations performed by Turrini et al. (2011) (see Figs. 6 and 7 and Turrini 2014; Turrini & Svetsov 2014 for more details on the distribution of the impact velocities in the different migration scenarios).

We performed simulations of cometary impactors composed by a homogeneous mixture of rocks and ices (see Svetsov and Shuvalov 2015, Fig. 5). Among the materials supplied by the ANEOS equations of state (Thompson and Lauson, 1972), we adopted water as our template for the icy component and granite as our template for the rocky one. The simulations described in Turrini et al. (2016) provided us with analogous results for asteroidal rocky

766 impactors.

767 Among the different kinds of rocky impactors (granite impactors, dunite
768 impactors and differentiated impactors) simulated by Turrini et al. (2016)
769 we adopted their results for granite impactors as our template for asteroidal
770 impactors. The comparison between the results of impact experiments (Hol-
771 sapple, 1993; Holsapple and Housen, 2007; Daly and Schultz, 2016) and those
772 of SOVA's simulations reveals that they agree within a factor of two (Svetsov,
773 2011; Turrini et al., 2016).

774 4.5.1. Mass loss associated to the impact events

775 Following Turrini (2014) and Turrini & Svetsov (2014), we defined three
776 classes of impact events based on their normalized specific energy Q_D/Q_D^* ,
777 where Q_D^* is the catastrophic disruption threshold of Vesta. Impacts with
778 $Q_D/Q_D^* < 0.1$ were classified as *low-energy impacts*. Impacts with $0.1 \leq$
779 $Q_D/Q_D^* < 1$ were classified as *high-energy impacts*. Impacts with $Q_D/Q_D^* \geq 1$
780 were classified as *catastrophic impacts*.

781 The quantity Q_D^* was computed using Eq. 6 from Benz and Asphaug
782 (1999) with the associated coefficients for basaltic targets (see Table 3, Benz
783 and Asphaug 1999). Following Turrini (2014) and Turrini & Svetsov (2014),
784 we used the coefficients of the case $v_i = 5 \text{ km s}^{-1}$ for impacts with velocity
785 greater or equal than 5 km s^{-1} , and those of the case $v_i = 3 \text{ km s}^{-1}$ for all
786 the other impacts.

787 We computed the mass loss associated to low-energy impacts using the
788 results of the impact simulations with SOVA performed in the framework of
789 this study and those performed by Turrini et al. (2016). The results of the
790 simulations are shown in Fig. 8, where the mass loss as a function of the

791 impact velocity is expressed in units of the mass of the impacting body. For
792 comparison, in Fig. 8 we also plotted the results of the simulations by Turrini
793 & Svetsov (2014) for cometary impactors composed of pure water ice.

794 For high-energy impacts we used instead Eq. 8 from Benz and Asphaug
795 (1999) expressed in terms of the eroded mass:

$$\frac{m_e}{m_t} = 0.5 + s \left(\frac{Q_D}{Q_D^*} - 1.0 \right) \quad (4)$$

796 where $s = 0.5$ for $v_i < 5 \text{ km s}^{-1}$ and $s = 0.35$ for $v_i \geq 5 \text{ km s}^{-1}$. To avoid
797 overestimating the contribution of high-energy impacts to Vesta's crustal ero-
798 sion, the effects of those high-energy impact events that, after renormalizing
799 to the appropriate SFD, were associated to less than one real impact were
800 not considered in estimating Vesta's crustal erosion.

801 The effects of catastrophic impacts were not accounted for in the esti-
802 mates of the eroded mass: their cumulative number was used only to assess
803 the probability of Vesta surviving its primordial collisional evolution without
804 being shattered (see also Turrini 2014; Turrini & Svetsov 2014 for a discus-
805 sion).

806 4.5.2. Mass gain associated to the impact events

807 To assess the mass accretion experienced by primordial Vesta we again
808 took advantage of the results of the impact simulations with SOVA performed
809 in the framework of this study and those performed by Turrini et al. (2016).
810 The results of the simulations are shown in Fig. 9, where the accreted mass
811 as a function of the impact velocity is expressed in units of the mass of the
812 impacting body. For comparison, in Fig. 9 we also plotted the results of the
813 simulations by Turrini & Svetsov (2014) for cometary impactors composed

814 of pure water ice.

815 The results of the simulations in Turrini et al. (2016) indicated that the
 816 composition and the diameter of rocky impactors do not change the results
 817 of the simulations as much as the impact velocity (i.e. the effects of the
 818 former parameters are limited to about 5 – 10%, see Turrini et al. 2016 for a
 819 discussion). Both low-energy and high-energy ones contributed mass to Vesta
 820 according to the results shown in Fig. 9, while catastrophic impact did not
 821 contribute mass to Vesta. For consistency with the procedure adopted in
 822 estimating the mass loss caused by high-energy impacts, the contribution of
 823 those high-energy impact events that, after renormalizing to the appropriate
 824 SFD, were associated to less than one real impact was not considered in
 825 estimating Vesta’s late accretion.

826 5. Results

827 In the following we present the late accretion and erosion experienced by
 828 Vesta’s crust across Jupiter’s formation and migration, as depicted by our
 829 results taken at face value. For each of the four SFDs we considered we will
 830 show the average mass loss, mass accretion and water accretion produced
 831 by Vesta’s early collisional evolution. We will first discuss the separate con-
 832 tributions of asteroidal and cometary impactors, which are defined as those
 833 planetesimals originating within and beyond 4 au respectively, and then their
 834 cumulative effects on Vesta. When considering the cumulative collisional his-
 835 tory of the asteroid, we will discuss how it affects both a primordial Vesta
 836 similar in mass to the present one (“*intact and pristine Vesta*” scenario) and
 837 a Vesta two to three times larger (“*altered Vesta*” scenario).

For each of the average quantities we computed, we will also show the associated standard deviations as a measure of the variability of our results. The two main factors affecting the magnitude of the standard deviations are the total flux of impactors and the variability of the number of the largest impactors (see e.g. Turrini et al. 2014, 2016). As such, the largest standard deviations will be associated to the populations of cometary impactors (more affected by the effects of small-number statistics due to their lower fluxes) and to the population of collisionally-evolved impactors formed in turbulent discs (due to the effects of small-number statistics on the flux of large impactors).

5.1. Mass loss and crustal erosion

The first step of our analysis focused on the mass loss suffered by primordial Vesta in the classical “intact and pristine Vesta” scenario, where the asteroid always possessed a mass similar to its present one. The mass loss caused by asteroidal and cometary impactors individually is shown in Fig. 10 and is dominated by the effects of low-energy impacts (see also Turrini 2014; Turrini & Svetsov 2014). Catastrophic impacts have a limited probability to occur (generally less than 0.1% and never above 1%).

High-energy impacts are comparatively more probable in the case of the SFDs associated with a turbulent circumsolar disc. Also in those cases, however, the chances of high-energy impacts occurring never exceed 20–30%. The only notable exception is the case of primordial planetesimals formed in a turbulent circumsolar disc (Chambers, 2010) when Jupiter migrates by 1 au, where Vesta could experience two high-energy impacts (responsible for about 60% of the total mass loss associated to this SFD in this migration

scenario).

The mass loss experienced by Vesta due to asteroidal impactors (Fig. 10, left panel) is limited in the cases of no migration or 0.25 au of migration of Jupiter but experiences a rapid growth once Jupiter's migration reaches and exceeds 0.5 au. The initial limited mass loss, of the order of $\sim 1\%$, is mainly due to impactors excited by the 3:1 resonance with Jupiter. When Jupiter's migration reaches 0.5 au a second family of higher-velocity impactors excited by the 2:1 resonance with Jupiter appears (see Fig. 1 and Turrini et al. 2011). This second family causes the mass loss experienced by Vesta to grow by about an order of magnitude.

The mass loss associated to cometary impactors shows an opposite trend, being significant only when Jupiter does not experience migration and dropping by more than one order of magnitude in those scenarios where the giant planet migrates (see Fig. 10, right panel). This is due to the fact that the migration of the giant planet favours the trapping of more and more planetesimals in the sweeping resonances at the outer boundaries of the asteroid belt, reducing Jupiter's efficiency in scattering cometary planetesimals in the orbital region of Vesta (see Fig. 1 and Turrini et al. 2011).

The total mass loss experienced by Vesta in the different scenarios is shown in Fig. 11. As can be immediately seen, the order of magnitude of the mass loss experienced by Vesta is mainly a function of Jovian migration. The actual SFD of the impacting planetesimals appears to affect the result, within a given migration scenario, to roughly a factor of three. Fig. 11 reveals that the most favourable cases in terms of experienced mass loss and preservation of the vestan crust are that of a Jovian displacement of 0.25 au

888 and that of no migration of the giant planet.

889 The cases of a Jovian migration of 0.5 and 1 au appear less favourable
 890 and, for a primordial Vesta characterized by a mass similar to its present
 891 one, they appear inconsistent with the survival of Vesta's crust (especially
 892 once the excavation caused by the two vestan South polar impact basins is
 893 taken into account). The case of a Jovian migration of 1 au, in particular,
 894 is associated to a mass loss of the same order as the expected mass of the
 895 vestan crust.

896 We then moved to investigate how the picture depicted by these results
 897 would change in the "altered Vesta" scenario, where primordial Vesta is hy-
 898 pothesized to have been more massive than its present counterpart (Consol-
 899 magno et al., 2015). For a primordial Vesta twice as massive as present Vesta,
 900 the radius of the asteroid would be larger by about 25% than the present one
 901 and the escape velocity would increase by about 100 m/s, i.e about 30%. The
 902 increase in the escape velocity would lower the average efficiency of impacts
 903 in causing mass loss by about 30% (see Eq. 3 in Svetsov 2011). As the flux
 904 of impactors on Vesta is directly proportional to the radius of the asteroid,
 905 the increase in the radius would translate into a similar increase in the flux
 906 of impactors (see Turrini et al. 2011 for details). The new flux almost com-
 907 pensates for the decrease in the erosion efficiency of the impacts, so that the
 908 overall erosion decreases by about 10%.

909 Because of this, the values plotted in Figs. 10 and 11 would scale down
 910 by slightly more than the mass ratio between the primordial Vesta and the
 911 present one. For a primordial Vesta twice as massive as the present one, these
 912 values would decrease by a factor of two. The only scenario incompatible with

the constraint on Vesta’s mass loss would become that of a Jovian migration of 1 au (either due to the mass loss per se or to its combination with the later excavation caused by the South polar basins).

A larger primordial mass of Vesta would proportionally decrease the mass lost by the asteroid due to collisions. For a primordial Vesta three times as massive as the present one (see Fig. 11), the only cases that would be rejected by the constraint on the crustal survival would be those where Jupiter migrated by 1 au and the flux of impactors on Vesta was dominated by planetesimals with diameters larger than 10 km, as in the SFDs by Coradini et al. (1981) and Chambers (2010).

5.2. Mass accretion and water delivery

As discussed in Sects. 3 and 4, the impacts on Vesta would also cause the asteroid to experience a phase of late accretion. The second step of our analysis was to quantify how much water would be delivered to Vesta by the two potential sources we considered, volatile-rich asteroids and ice-rich comets (see Sects. 3 and 4), and compare the estimated amounts with the upper bound set by the presence of apatites in basaltic eucrites. Again, we started with the classical “intact and pristine Vesta” scenario, where the asteroid always possessed a mass similar to its present one.

The individual contributions of asteroids and comets are shown in Fig. 12. Asteroidal impactors (Fig. 12, left panel) deliver water to Vesta only when the Jovian migration reaches or exceeds 0.5 au, as the dynamical excitation of the population of planetesimals affected by the sweeping 2:1 resonance with Jupiter allows them to reach the orbital region of Vesta and deliver water to the asteroid (see Fig. 1 and Turrini et al. 2011).

938 The case of cometary impactors (Fig. 12, right panel) is opposite to
 939 that of the asteroidal ones, as they deliver significant amounts of water to
 940 Vesta only when Jupiter does not migrate. If the giant planet migrates, the
 941 amount of water accreted by Vesta drops by more than one order of mag-
 942 nitude, showing however a slowly increasing trend with increasing displace-
 943 ments of Jupiter. The SFD associated to primordial planetesimals formed in
 944 a turbulent circumstellar disc (see Sect. 4.3.2) does not appear in the right
 945 panel of Fig. 12 as its total flux amounts to less than one impact event.

946 The cumulative water enrichments produced by asteroidal and cometary
 947 impactors in the different migration scenarios for Jupiter are shown in Fig.
 948 13, where they are compared with the range of values for Vesta's water
 949 mass fraction derived from the estimates of Stephant et al. (2016a,b) and
 950 Sarafian et al. (2017a,b). The cases where Jupiter migrated by 0.5 au or
 951 more appear inconsistent with the observational data, as the volatile-rich
 952 asteroidal impactors would produce a water enrichment from a few times to
 953 an order of magnitude larger.

954 The case of no migration of Jupiter also shows inconsistencies with the
 955 observational data, but in this case the inconsistencies appear to be also SFD-
 956 dependent. Collisionally evolved SFDs produce water enrichments greater
 957 than the ranges of values derived from the estimates of Stephant et al.
 958 (2016a,b) and Sarafian et al. (2017a,b) while primordial SFDs are associated
 959 to lower ones. In the case of primordial planetesimals formed in quiescent
 960 discs the produced water enrichment is just below the range of values derived
 961 from eucrites, while in the extreme case of primordial planetesimals formed
 962 in a turbulent circumsolar disc no water enrichment is produced (beyond

Vesta's initial water budget, if different from zero).

As in the case of mass loss, we tested how these results would change in the “altered Vesta” scenario, where primordial Vesta is hypothesized to have been more massive than its present counterpart (Consolmagno et al., 2015). If we consider again a primordial Vesta twice as massive as present Vesta, the increase in the escape velocity should increase the average efficiency of impacts in delivering water by about 5% (see Eq. 8 in Svetsov 2011). At the same time, the increase in the radius would translate in a proportional increase in the flux of impactors.

Therefore, a larger primordial Vesta would accrete material more efficiently from a larger number of bodies, partially counteracting the drop in the water enrichment caused by the increase in the crustal mass over which to distribute the accreted water. As a result, the values shown in Figs. 12 and 13 would decrease only by about 33% for a primordial Vesta twice as massive as the present one. For a primordial Vesta three times as massive as the present one, the decrease would amount to about 50%.

As one can see from Fig. 13, such a decrease does not qualitatively change the outcome of our earlier analysis. Jovian displacements of 0.5 au or larger would still be inconsistent with the constraint posed by the water enrichment of eucrites. Likewise, a lack of migration by Jupiter would be inconsistent with said constraint for collisionally evolved SFDs of the impactors dominated in number by planetesimals smaller than about 10 km (as in the SFDs by Weidenschilling 2011 and Morbidelli et al. 2009).

5.3. Mass accretion and HSEs enrichment

The final step of our analysis was to compare the effects of the global accretion of chondritic material experienced by Vesta with the HSEs enrichment of diogenites, starting also in this case with the classical “intact and pristine Vesta” scenario, where the asteroid always possessed a mass similar to its present one. In computing such accretion we considered, alongside with the contribution of asteroidal impactors, that of the non-ice component of the cometary impactors (see Sect. 4.3). The individual contributions of asteroidal and cometary impactors are shown in Fig. 14.

The accretion of chondritic material associated to asteroidal impactors (Fig. 14, left panel) increases proportionally to Jupiter’s displacement due to the growing flux of impactors experienced by Vesta (Turrini et al., 2011). The accretion associated to cometary impactors (Fig. 14, right panel) follows the same pattern seen when discussing the accretion of water (see Fig. 12, right panel) and proves marginal with respect to that of asteroidal impactors.

The overall late accretion experienced by Vesta is shown in Fig. 15 and immediately reveals two striking features. The first one is that planetesimals formed in a turbulent circumsolar disc, independently on them being primordial or collisionally evolved, appear to be not consistent with the constraint posed by the HSEs enrichment of diogenites. The second one is that in general the mass accretion experienced by a primordial Vesta with mass similar to that of the present Vesta appears to be at most marginally consistent with said constraint.

In the cases of limited (0.25 au) and no migration, planetesimals formed in quiescent discs produce a mass accretions of about 1% of the vestan mass

1011 while those formed in turbulent discs produce a mass accretions of about 2%.
 1012 In the cases of moderate (0.5 au) and large (1 au) migration, the resulting
 1013 mass accretion is of about 2% of the vestan mass or larger for all kinds of
 1014 impactors. As we discussed in Sect. 3, while Day et al. (2012) estimated the
 1015 accreted mass to fall between 1% and 2% of the mass of Vesta, we treated
 1016 this range of values as an upper limit in this study to account for the uncer-
 1017 tainties on the interpretation of the diogenitic data and for the fact that the
 1018 process we are considering lasted only a fraction of the total time over which
 1019 diogenites can be enriched in HSEs by impacts (see Sect. 3).

1020 For a primordial Vesta with a mass similar to the present one of the aster-
 1021 oid, therefore, the cases that best fit the HSEs data among those considered
 1022 here are those of no or limited (0.25 au) migration of Jupiter in a quiescent
 1023 circumsolar disc. Even these cases, however, produce an enrichment reaching
 1024 the lower end of the range identified by Day et al. (2012). We therefore tested
 1025 the behaviour of the accretion of chondritic mass in the “altered Vesta” sce-
 1026 nario considering a primordial Vesta twice or three times larger than the
 1027 present one.

1028 Applying the same scaling discussed for water accretion to the values
 1029 shown in Fig. 15, we can see that a primordial Vesta two to three times
 1030 more massive than the present Vesta (see Fig. 15) would make planetesimals
 1031 formed in turbulent discs (like in the SFDs by Chambers 2010 and Morbidelli
 1032 et al. 2009) more consistent with the HSEs constraint in the scenarios of
 1033 limited (0.25 au) or no migration of Jupiter. At the same time, it would make
 1034 the case of collisionally evolved planetesimals formed in quiescent discs (like
 1035 the SFD by Weidenschilling 2011) more consistent with the HSEs constraint

also for a moderate displacement (0.5 au) of Jupiter.

6. Discussion and conclusions

The goal we set for ourselves in this work was to investigate whether the erosional and accretional history of the primordial Vesta as recorded by the HEDs can be used to probe into the early collisional history of asteroid Vesta and, through that, into the early evolution of the Solar System. Before discussing the results we obtained, however, we emphasize once again that they should be considered only as illustrative (or just as a more refined back-of-the-envelope calculation) since some of the approximations adopted in our proof-of-concept case study were motivated only by reasons of convenience and neglected important processes, like gas drag, that should be included in future more physically complete investigations. Because of this, in the following we will limit ourselves to discussing the general trends we observed in our results.

Notwithstanding its limitations, the proof-of-concept case study we investigated appears to indicate that the three compositional characteristics of Vesta and the HEDs we considered in this work (namely, the survival of Vesta's basaltic crust, the enrichment in water of eucrites and the enrichment in HSEs of diogenites) offer complementary pieces of information that, once considered together, provide stronger constraints than when considered individually. Moreover, the constraints they provide only rely on the assumption of a chondritic bulk composition of Vesta in terms of its major rock-forming elements and, as the comparison between the "intact and pristine Vesta" scenario and the "altered Vesta" scenario highlights, they appear to be limitedly

1060 influenced by the proposed uncertainty on Vesta's primordial mass.

1061 In our proof-of-concept case study the crustal survival to cratering erosion
 1062 allows to reject only the case of a Jovian migration of 1 au. The constraint
 1063 offered by the survival of Vesta's basaltic crust to cratering erosion would
 1064 therefore appear to be the least powerful among those we investigated, as
 1065 the information it provides is already contained **within** that provided by
 1066 the two constraints associated to late accretion. The accretion history of the
 1067 primordial Vesta appears instead to provide stronger constraints: both water
 1068 accretion and mass accretion agree in rejecting the cases of Jovian migration
 1069 of 0.5 and 1 au, with water accretion also indicating that the case of no
 1070 migration of the giant planet is inconsistent with the HEDs data, particularly
 1071 if the D/H ratio of the planetesimal population represented by our cometary
 1072 impactors was inconsistent with that reported for Vesta's source of water
 1073 (Sarafian et al., 2014).

1074 Among the three constraints, water accretion appears more sensitive to
 1075 the effects of Jupiter's migration, effectively pinpointing it to about 0.25 au
 1076 among the simplified cases considered. Mass accretion appears more capable
 1077 of discriminating between the effects of different size distributions of the im-
 1078 pacting planetesimals, favouring the collisionally-evolved SFDs in contrast to
 1079 primordial ones and the SFDs associated to quiescent nebular environments
 1080 in contrast to those associated to turbulent nebular environments. Notwith-
 1081 standing its apparent weakness, the survival of Vesta's basaltic crust remains
 1082 an important constraint when studying more violent collisional scenarios **than**
 1083 those here considered.

1084 Specifically, the collisional evolution of the primordial Vesta in those sce-

1085 narios dominated by high-velocity or even high-energy impacts (e.g. the
 1086 so-called “Grand Tack”, Walsh et al. 2011; O’Brien et al. 2014) will be deter-
 1087 mined by mass loss without mass accretion playing a significant role. This
 1088 leading role of mass loss will be particularly true for scenarios invoking a
 1089 major role of “hit-and-run” collisions, like those suggested to be responsible
 1090 for the “altered Vesta” scenario (Consolmagno et al., 2015), in the collisional
 1091 evolution of the inner Solar System, as in those cases the contribution of said
 1092 impacts to mass accretion will be null or negligible.

1093 It should be noted, moreover, that in case of stochastic large impacts it
 1094 is possible for a scenario to be characterized by a moderate or even limited
 1095 global crustal erosion but a large local excavation. This is indeed the case
 1096 of the last 4 Gyr of collisional evolution of Vesta, where the total crustal
 1097 erosion was limited to about 30 m but the impacts that produced Veneneia
 1098 and Rheasilvia locally excavated tens of km. As proposed in Turrini et al.
 1099 (2011) and further discussed in Turrini (2014) and Turrini & Svetsov (2014),
 1100 impacts of this kind occurring on primordial Vesta could cause effusive events
 1101 where the magma originates from the mantle and could in principle produce
 1102 compositional signatures in Vesta’s crust incompatible with Dawn’s measure-
 1103 ments. Given the degree of collisional remixing of Vesta’s crust suggested by
 1104 Dawn’s observations (De Sanctis et al., 2012; Prettyman et al., 2012), these
 1105 scenarios should be investigated on a case-by-case basis if they can success-
 1106 fully pass the test on the global crustal survival. It is interesting to note,
 1107 however, that those scenarios that could produce the excavation or effusion
 1108 of mantle material in Turrini (2014) and Turrini & Svetsov (2014) are among
 1109 those rejected by the three constraints.

1110 The scenarios we considered in our proof-of-concept case study represent
 1111 only a limited subset of all proposed evolutionary tracks for the early Solar
 1112 System. As an example, it has been proposed that Vesta could have formed
 1113 on an inner orbit located between the orbit of Mars and the inner edge of
 1114 asteroid belt (Bottke et al., 2006) instead of in the inner asteroid belt. It
 1115 is also possible for the giant planets to have undergone a more extensive
 1116 migration than that considered in this work (Walsh et al., 2011; Bitsch et
 1117 al., 2015). This extensive migration, in turn, could have kept them in the
 1118 outer Solar System (Bitsch et al., 2015) or could have brought them to cross
 1119 the inner Solar System (Walsh et al., 2011). All these different possibilities
 1120 will be associated to different fluxes of impactors on Vesta and will need to be
 1121 tested case by case against the three astrochemical constraints we identified.

1122 Also the scenarios we considered for primordial Vesta do not exhaust all
 1123 the different possibilities. As an example, it has been proposed that a slower
 1124 formation of Vesta could cause the heat released by the short-lived radioac-
 1125 tive elements not to be enough to melt the conductive lid of the asteroid,
 1126 which would preserve its original undifferentiated composition (Formisano
 1127 et al., 2013). This undifferentiated crust would be reprocessed over time by
 1128 the effusive processes responsible for the creation of Vesta's basaltic crust, as
 1129 discussed in Sect. 3, and could therefore represent a source of HSEs and pos-
 1130 sibly water for the vestan magma, whose effects on the enrichment of eucrites
 1131 and diogenites need to be verified against the astrochemical constraints on
 1132 Vesta's late accretion.

1133 Finally, the temporal interval covered by our proof-of-concept case study
 1134 spans only a fraction of the temporal windows (see Sect. 3) over which Vesta's

1135 crust can be compositionally altered or eroded by impacts: later events,
 1136 therefore, are also expected to leave their marks on Vesta and the HEDs. In
 1137 particular, in the scenarios we investigated it is expected that, after Jupiter's
 1138 formation, the interplay between the gravitational perturbations of the giant
 1139 planet and those of the planetary embryos embedded into the primordial
 1140 asteroid belt will start a phase of dynamical excitation and clearing of the
 1141 belt itself (Wetherill, 1992; Petit, Morbidelli & Chambers, 2001; O'Brien,
 1142 Morbidelli & Bottke, 2007), changing its orbital structure to its present one
 1143 (albeit with a larger population of asteroids). Planetesimals impacting Vesta
 1144 during this phase of dynamical excitation and clearing will also contribute
 1145 to the mass accretion and mass loss histories of the asteroid and their effects
 1146 will cumulate with those of the Jovian Early Bombardment.

1147 Applying the three astrochemical constraints we investigated to a more
 1148 deterministic study of the history of the early Solar System is beyond the
 1149 scope of our proof-of-concept case study and is left to future works based on
 1150 a more complete physical model and spanning longer temporal intervals. In
 1151 particular, future works will need to include the effects of gas drag, which
 1152 will change both the flux of impactors on Vesta and the distribution of the
 1153 impact velocities, and of the population of planetary embryos embedded
 1154 into the planetesimal disk, which is expected to both dynamically excite the
 1155 planetesimals and start a process of depletion of the asteroid belt once Jupiter
 1156 has completed its formation (the latter process becoming more efficient in
 1157 case of an eccentric orbit of the forming Jupiter), in assessing the collisional
 1158 evolution of primordial Vesta.

1159 In conclusion, the main result of this work is the identification of the

constraints offered by eucrites and diogenites and the showcasing of their joint use as a window into the ancient past of the Solar System. Our take home message can be summarized by the following “Lather, Rinse, Repeat” recipe for future studies. Pick the scenario for Vesta that you consider most realistic, put it into the scenario for the evolution of the early Solar System that you want to investigate, and include all the necessary physical ingredients. Let it evolve and check if Vesta’s resulting accretional and erosional histories are consistent with the global constraints offered by eucrites and diogenites. Start over as many time as needed.

Acknowledgements

The authors wish to thank Miroslav Brož, an anonymous referee, Chris Russell and the whole Dawn team. This research has been supported by the Italian Space Agency (ASI) and by the International Space Science Institute (ISSI) in Bern through the International Teams 2012 project “Vesta, the key to the origins of the Solar System” (www.issibern.ch/teams/originsolsys). The computational resources used in this research have been supplied by INAF-IAPS through the projects “HPP - High Performance Planetology” and “DataWell.”

References

- Ammannito, E., and 21 colleagues 2013. Olivine in an unexpected location on Vesta’s surface. *Nature* 504, 122-125.
- Barrett, T. J., Barnes, J. J., Tartèse, R., Anand, M., Franchi, I. A., Greenwood, R. C., Charlier, B. L. A., Grady, M. M. 2016. The abundance and

- isotopic composition of water in eucrites. *Meteoritics and Planetary Science* 51, 1110-1124.
- Benz, W., Asphaug, E. 1999. Catastrophic Disruptions Revisited. *Icarus* 142, 5-20.
- Bitsch B., Lambrechts M., Johansen A. 2015. The growth of planets by pebble accretion in evolving protoplanetary discs. *Astronomy and Astrophysics* 582, article id. A112.
- Bizzarro, M., Baker, J. A., Haack, H., Lundgaard, K. L. 2005. Rapid Timescales for Accretion and Melting of Differentiated Planetesimals Inferred from ^{26}Al - ^{26}Mg Chronometry. *The Astrophysical Journal* 632, L41-L44.
- Bottke W. F., Nesvorný D., Grimm R. E., Morbidelli A., O'Brien D. P. 2006. Iron meteorites as remnants of planetesimals formed in the terrestrial planet region. *Nature* 439, 821-824.
- Bouvier, A., Wadhwa, M. 2010. The age of the Solar System redefined by the oldest Pb-Pb age of a meteoritic inclusion. *Nature Geoscience* 3, 637-641.
- Britt, D. T., Yeomans, D., Housen, K., Consolmagno, G. 2002. Asteroid Density, Porosity, and Structure. *Asteroids III* 485-500.
- Brož, M., Morbidelli, A., Bottke, W. F., Rozehnal, J., Vokrouhlický, D., Nesvorný, D. 2013. Constraining the cometary flux through the asteroid belt during the late heavy bombardment. *Astronomy and Astrophysics* 551, A117.

- 1205 Carry, B. 2012. Density of asteroids. *Planetary and Space Science* 73, 98-118.
- 1206 Chambers, J. E. 2010. Planetesimal formation by turbulent concentration.
1207 *Icarus* 208, 505-517.
- 1208 Clenet, H., Jutzi, M., Barrat, J.-A., Asphaug, E. I., Benz, W., Gillet, P.
1209 2014. A deep crust-mantle boundary in the asteroid 4 Vesta. *Nature* 511,
1210 303-306.
- 1211 Consolmagno, G. J., Drake, M. J. 1977. Composition and evolution of the
1212 eucrite parent body - Evidence from rare earth elements. *Geochimica et*
1213 *Cosmochimica Acta* 41, 1271-1282.
- 1214 Consolmagno, G. J., Golabek, G. J., Turrini, D., Jutzi, M., Sirono, S.,
1215 Svetsov, V., Tsiganis, K. 2015. Is Vesta an intact and pristine protoplanet?.
1216 *Icarus* 254, 190-201.
- 1217 Consolmagno G. J., Rubie D. C. and Golabek G. J., 2016. The grand tack,
1218 Vesta, and the missing olivine problem. *Meteoritical Society annual meet-*
1219 *ing abstract n. 6066.*
- 1220 Coradini, A., Magni, G., Federico, C. 1981. Formation of planetesimals in an
1221 evolving protoplanetary disk. *Astronomy and Astrophysics* 98, 173-185.
- 1222 Coradini, A., Magni, G., Turrini, D. From gas to satellitesimals: Disk for-
1223 mation and evolution. *Space Sci. Rev.* 153, 411-429.
- 1224 Coradini, A., Turrini, D., Federico, C., Magni, G. 2011. Vesta and Ceres:
1225 Crossing the History of the Solar System. *Space Science Reviews* 163, 25-
1226 40.

- 1227 Cuzzi, J. N., Hogan, R. C., Shariff, K. 2008. Toward Planetesimals: Dense
1228 Chondrule Clumps in the Protoplanetary Nebula. *The Astrophysical Jour-*
1229 *nal* 687, 1432-1447.
- 1230 Cuzzi, J. N., Hogan, R. C., Bottke, W. F. 2010. Towards initial mass func-
1231 tions for asteroids and Kuiper Belt Objects. *Icarus* 208, 518-538.
- 1232 D'Angelo G., Durisen R. H., Lissauer J. J. Giant Planet Formation. In *Exo-*
1233 *planets*; edited by S. Seager. University of Arizona Press: Tucson, Arizona,
1234 2011, pp. 319-346.
- 1235 Dale, C. W., Burton, K. W., Greenwood, R. C., Gannoun, A., Wade, J.,
1236 Wood, B. J., Pearson, D. G. 2012. Late Accretion on the Earliest Plan-
1237 etesimals Revealed by the Highly Siderophile Elements. *Science* 336, 72.
- 1238 Davis, D. R., Chapman, C. R., Greenberg, R., Weidenschilling, S. J., Harris,
1239 A. W. 1979. Collisional evolution of asteroids - Populations, rotations, and
1240 velocities. *Asteroids* 528-557.
- 1241 Davis, D. R., Chapman, C. R., Weidenschilling, S. J., Greenberg, R. 1985.
1242 Collisional history of asteroids: Evidence from Vesta and the Hirayama
1243 families. *Icarus* 62, 30-53.
- 1244 Day, J. M. D., Walker, R. J., Qin, L., Rumble, D., III 2012. Late accretion as
1245 a natural consequence of planetary growth. *Nature Geoscience* 5, 614-617.
- 1246 Day J. M. D., Brandon A. D., Walker, R. J., 2016. Highly Siderophile Ele-
1247 ments in Earth, Mars, the Moon, and Asteroids. *Reviews in Mineralogy &*
1248 *Geochemistry* 81, 161-238

- 1249 Daly, R.T., Schultz, P.H., 2016. Delivering a projectile component to the
1250 vestan regolith. *Icarus* 264, 9-19.
- 1251 De Sanctis, M. C., and 22 colleagues 2012. Spectroscopic Characterization of
1252 Mineralogy and Its Diversity Across Vesta. *Science* 336, 697.
- 1253 DeMeo, F. E., Carry, B. 2014. Solar System evolution from compositional
1254 mapping of the asteroid belt. *Nature* 505, 629-634.
- 1255 Dhaliwal, J. K., Day, J. M. D., Tait, K. T. 2016. Establishing a Pristin-
1256 ity Index for Eucrites Using the Highly Siderophile Elements. *Lunar and*
1257 *Planetary Science Conference* 47, 2644.
- 1258 Dienes, J.K.; Walsh, J.M. Theory of Impact: Some General Principles
1259 and the Method of Eulerian Codes. In *High-Velocity Impact Phenomena*;
1260 Kinslow, R., Ed.; Academic Press: New York, NY, USA, 1970; pp. 46–104.
- 1261 Ermakov, A. I., Zuber, M. T., Smith, D. E., Raymond, C. A., Balmino, G.,
1262 Fu, R. R., Ivanov, B. A. 2014. Constraints on Vesta's interior structure
1263 using gravity and shape models from the Dawn mission. *Icarus* 240, 146-
1264 160.
- 1265 Lodders K. 2010. Solar System Abundances of the Elements. In: Goswami
1266 A., Reddy B. (eds) *Principles and Perspectives in Cosmochemistry. Astro-*
1267 *physics and Space Science Proceedings* 16. Springer, Berlin, Heidelberg,
1268 pp. 379-417.
- 1269 Fedele D., van den Ancker M. E., Henning Th., Jayawardhana R., Oliveira
1270 J. M., 2010. Timescale of mass accretion in pre-main-sequence stars. *As-*
1271 *tronomy and Astrophysics* 510, id. A72.

- 1272 Formisano, M., Federico, C., Turrini, D., Coradini, A., Capaccioni, F., De
1273 Sanctis, M. C., Pauselli, C. 2013. The heating history of Vesta and the
1274 onset of differentiation. *Meteoritics and Planetary Science* 48, 2316-2332.
- 1275 Goldreich, P., Ward, W. R. 1973. The Formation of Planetesimals. *The As-*
1276 *trophysical Journal* 183, 1051-1062.
- 1277 Grazier, K. R., Castillo-Rogez, J. C., Sharp, P. W. 2014. Dynamical delivery
1278 of volatiles to the outer main belt. *Icarus* 232, 13-21.
- 1279 Greenwood, R. C., Barrat, J.-A., Yamaguchi, A., Franchi, I. A., Scott,
1280 E. R. D., Bottke, W. F., Gibson, J. M. 2014. The oxygen isotope compo-
1281 sition of diogenites: Evidence for early global melting on a single, compo-
1282 sitionally diverse, HED parent body. *Earth and Planetary Science Letters*
1283 390, 165-174.
- 1284 Hartogh, P., Lis, D.C., Bockelée-Morvan, D., de Val-Borro, M., Biver, N.,
1285 Küppers, M., Emprechtinger, M., Bergin, E.A., Crovisier, J., Rengel, M.,
1286 et al (2011). Ocean-like water in the Jupiter-family comet 103P/Hartley
1287 2. *Nature* 478, 218-220.
- 1288 Holsapple, K. A. 1993. The scaling of impact processes in planetary sciences.
1289 *Annual Review of Earth and Planetary Sciences* 21, 333-373.
- 1290 Holsapple, K. A., Housen, K. R. 2007. A crater and its ejecta: An interpre-
1291 tation of Deep Impact. *Icarus* 187, 345-356.
- 1292 Ivanov, B. A., Melosh, H. J., 2013. Two-dimensional numerical modeling of
1293 the Rheasilvia impact formation. *J. Geophys. Res.* 118, 1545-1557.

- 1294 Jarosewich, E. 1990. Chemical analyses of meteorites - A compilation of stony
1295 and iron meteorite analyses. *Meteoritics* 25, 323-337.
- 1296 Johnson B. C., Walsh K. J., Minton D. A., Krot A. N., Levison H. L. (2016).
1297 Timing of the formation and migration of giant planets as constrained by
1298 CB chondrites. *Science Advances* 2, art. id. e1601658, DOI: 10.1126/sci-
1299 adv.1601658.
- 1300 Jutzi, M., Asphaug, E., Gillet, P., Barrat, J.-A., Benz, W. 2013. The struc-
1301 ture of the asteroid 4 Vesta as revealed by models of planet-scale collisions.
1302 *Nature* 494, 207-210.
- 1303 Kruijer, T. S., Burkhardt, C., Budde, G., Kleine, T. 2017. Age of Jupiter
1304 inferred from the distinct genetics and formation times of meteorites. *Pro-
1305 ceedings of the National Academy of Science* 114, 6712-6716.
- 1306 Lissauer, J.J., Hubickyj, O., D'Angelo, G., Bodenheimer, P. Models of
1307 Jupiter's growth incorporating thermal and hydrodynamic constraints.
1308 *Icarus* 199, 338-350.
- 1309 Mandler, B. E., Elkins-Tanton, L. T. 2013. The origin of eucrites, diogenites,
1310 and olivine diogenites: Magma ocean crystallization and shallow magma
1311 chamber processes on Vesta. *Meteoritics and Planetary Science* 48, 2333-
1312 2349.
- 1313 McCord, T. B., Adams, J. B., Johnson, T. V. 1970. Asteroid Vesta: Spectral
1314 Reflectivity and Compositional Implications. *Science* 168, 1445-1447.
- 1315 McSween H. Y., Mittlefehldt D. W., Beck A. W., Mayne R. G., and McCoy

- 1316 T. J. 2011. HED meteorites and their relationship to the geology of Vesta
1317 and the Dawn Mission. *Space Science Reviews* 163, 141-174
- 1318 Melosh, H.J., 1989. *Impact Cratering: A Geologic Process*; Oxford Mono-
1319 graphs on Geology and Geophysics, No. 11; Oxford University Press: New
1320 York, NY, USA; p. 253.
- 1321 Michalak, G. 2000. Determination of asteroid masses — I. (1) Ceres, (2)
1322 Pallas and (4) Vesta. *Astronomy and Astrophysics* 360, 363-374.
- 1323 Michtchenko, T. A., Lazzaro, D., Carvano, J. M. 2016. On the current dis-
1324 tribution of main belt objects: Constraints for evolutionary models. *As-
1325 tronomy and Astrophysics* 588, A11.
- 1326 Moore W. B., Simon J. I., Alexander A., Webb G. (2017). Heat-pipes planets.
1327 *Earth and Planetary Science Letters* 474, 13-19.
- 1328 Morbidelli, A., Bottke, W. F., Nesvorný, D., Levison, H. F. 2009. Asteroids
1329 were born big. *Icarus* 204, 558-573.
- 1330 Morbidelli A., Raymond S.N., 2016. Challenges in planet formation. *J. Geo-
1331 phys. Res. Planets* 121, 1962-1980.
- 1332 O'Brien D. P., Morbidelli A., Bottke W. F., 2007. The primordial excitation
1333 and clearing of the asteroid belt - Revisited. *Icarus* 191, 434-452
- 1334 O'Brien, D. P., Sykes, M. V. 2011. The Origin and Evolution of the Asteroid
1335 Belt - Implications for Vesta and Ceres. *Space Science Reviews* 163, 41-61.

- O'Brien, D. P., Walsh, K. J., Morbidelli, A., Raymond, S. N., Mandell, A. M.
2014. Water delivery and giant impacts in the Grand Tack scenario. *Icarus*
239, 74-84.
- Öpik, E. J. 1976. Interplanetary encounters: close-range gravitational in-
teractions. *Developments in solar system and space science* (Amsterdam
(Netherlands): Elsevier Scientific Publishing), 2, 7 + 155 p. .
- Petit J. M., Morbidelli A., Chambers J. E., 2001. The Primordial Excitation
and Clearing of the Asteroid Belt. *Icarus* 153, 338-347.
- Pierazzo, E.; Vickery, A.M.; Melosh, H.J., 1997. A reevaluation of impact
melt production. *Icarus* 127, 408-423.
- Pirani, S., Turrini, D. 2016. Asteroid 4 Vesta: Dynamical and collisional
evolution during the Late Heavy Bombardment. *Icarus* 271, 170-179.
- Prettyman, T. H., and 19 colleagues 2012. Elemental Mapping by Dawn
Reveals Exogenic H in Vesta's Regolith. *Science* 338, 242.
- Raymond, S. N., & Izidoro, A., 2017. Origin of water in the inner Solar
System: Planetesimals scattered inward during Jupiter and Saturn's rapid
gas accretion. *Icarus* 297, 134-148
- Robert, F. 2003. The D/H Ratio in Chondrites. *Space Science Reviews* 106,
87-101.
- Roszjar J., et al., 2016. Prolonged magmatism on 4 Vesta inferred from Hf-
W analyses of eucrite zircon. *Earth and Planetary Science Letters* 452,
216-226.

- 1358 Ruesch, O., and 14 colleagues 2014. Detections and geologic context of local
1359 enrichments in olivine on Vesta with VIR/Dawn data. *Journal of Geophys-*
1360 *ical Research (Planets)* 119, 2078-2108.
- 1361 Russell, C. T., and 27 colleagues 2012. Dawn at Vesta: Testing the Proto-
1362 planetary Paradigm. *Science* 336, 684.
- 1363 Russell, C. T., and 23 colleagues 2013. Dawn completes its mission at 4 Vesta.
1364 *Meteoritics and Planetary Science* 48, 2076-2089.
- 1365 Safronov, V. S. Evolution of the protoplanetary cloud and formation of the
1366 earth and planets. Nauka Press, 1969. Translated from Russian. Jerusalem
1367 (Israel): Israel Program for Scientific Translations, Keter Publishing
1368 House, 1972, pp. 212.
- 1369 Sarafian, A. R., Roden, M. F., Patiño-Douce, A. E. 2013. The volatile content
1370 of Vesta: Clues from apatite in eucrites. *Meteoritics and Planetary Science*
1371 48, 2135-2154.
- 1372 Sarafian, A. R., Nielsen, S. G., Marschall, H. R., McCubbin, F. M., Mon-
1373 teleone, B. D. 2014. Early accretion of water in the inner solar system from
1374 a carbonaceous chondrite-like source. *Science* 346, 623-626.
- 1375 Sarafian, A. R., Nielsen, S. G., Marschall, H. R., Gaetani, G. A., Hauri,
1376 E. H., Righter, K., Berger, E. L. 2017. Volatile Concentrations and H-
1377 Isotope Composition of Unequilibrated Eucrites. *Lunar and Planetary Sci-*
1378 *ence Conference* 48, 1436.
- 1379 Sarafian, A. R., John, T., Roszjar, J., Whitehouse, M. J. 2017. Chlorine and

- hydrogen degassing in Vesta's magma ocean. *Earth and Planetary Science Letters* 459, 311-319.
- Schenk, P., and 13 colleagues 2012. The Geologically Recent Giant Impact Basins at Vesta's South Pole. *Science* 336, 694.
- Scott, E. R. D. Meteoritical and dynamical constraints on the growth mechanisms and formation times of asteroids and Jupiter. *Icarus* 185, 72-82.
- Scott, E. R. D. 2007. Chondrites and the Protoplanetary Disk. *Annual Review of Earth and Planetary Sciences* 35, 577-620.
- Schiller, M., Baker, J., Creech, J., Paton, C., Millet, M.-A., Irving, A., Bizzarro, M. 2011. Rapid Timescales for Magma Ocean Crystallization on the Howardite-Eucrite-Diogenite Parent Body. *The Astrophysical Journal* 740, L22.
- Shuvalov, V.V. (1999) Multi-dimensional hydrodynamic code SOVA for interfacial flows: Application to thermal layer effect. *Shock Waves* 9, 381-390.
- Stephant, A., Hervig, R. L., Wadhwa, M. 2016. Water in Nominally Anhydrous Crustal Minerals of Vesta. *Lunar and Planetary Science Conference* 47, 2436.
- Stephant, A., Hervig, R., Bose, M., Wadhwa, M. 2016. D/H Ratios and Water Contents in Eucrite Minerals: Implications for the Source and Abundance of Water on Vesta. *LPI Contributions* 1921, 6212.
- Steenstra, E. S., Knibbe, J. S., Rai, N., van Westrenen, W. 2016. Constraints

- 1401 on core formation in Vesta from metal-silicate partitioning of siderophile
1402 elements. *Geochimica et Cosmochimica Acta* 177, 48-61.
- 1403 Svetsov, V. 2011. Cratering erosion of planetary embryos. *Icarus* 214, 316-
1404 326.
- 1405 Svetsov, V. V., Shuvalov, V. V. 2015. Water delivery to the Moon by aster-
1406 oidal and cometary impacts. *Planetary and Space Science* 117, 444-452.
- 1407 Thomas, P.C., Binzel, R.P., Gaffey, M.J., et al., 1997. Vesta: Spin pole, size,
1408 and shape from HST images. *Icarus* 128, 88-94.
- 1409 Thompson, S.L.; Lauson, H.S., 1972. Improvements in the Chart D
1410 Radiation-Hydrodynamic CODE III: Revised Analytic Equations of State;
1411 Report SC-RR-71 0714; Sandia National Laboratory: Albuquerque, NM,
1412 USA; p. 119.
- 1413 Tillotson, J.H., 1962. Metallic Equations of State for Hypervelocity Impact;
1414 General Atomic Report GA-3216; Advanced Research Project Agency:
1415 San Diego, CA, USA; p. 140.
- 1416 Toplis, M. J., and 10 colleagues 2013. Chondritic models of 4 Vesta: Impli-
1417 cations for geochemical and geophysical properties. *Meteoritics and Plan-*
1418 *etary Science* 48, 2300-2315.
- 1419 Tkalcic, B. J., Golabek G. J., Brenker F. E. 2013. Solid-state plastic deforma-
1420 tion in the dynamic interior of a differentiated asteroid. *Nature Geoscience*
1421 6, 93-97.

- 1422 Turrini, D., Magni, G., Coradini, A. 2011. Probing the history of Solar system
1423 through the cratering records on Vesta and Ceres. *Monthly Notices of the*
1424 *Royal Astronomical Society* 413, 2439-2466.
- 1425 Turrini, D., Coradini, A., Magni, G. 2012. Jovian Early Bombardment: Plan-
1426 etesimal Erosion in the Inner Asteroid Belt. *The Astrophysical Journal* 750,
1427 id. 8.
- 1428 Turrini, D. 2014. The primordial collisional history of Vesta: crater satura-
1429 tion, surface evolution and survival of the basaltic crust. *Planetary and*
1430 *Space Science* 103, 82-95.
- 1431 Turrini, D., Svetsov, V. 2014. The Formation of Jupiter, the Jovian Early
1432 Bombardment and the Delivery of Water to the Asteroid Belt: The Case
1433 of (4) Vesta. *Life* 4, 4-34.
- 1434 Turrini, D., and 12 colleagues 2014. The contamination of the surface of
1435 Vesta by impacts and the delivery of the dark material. *Icarus* 240, 86-102.
- 1436 Turrini, D., Nelson, R. P., Barbieri, M. 2015. The role of planetary formation
1437 and evolution in shaping the composition of exoplanetary atmospheres.
1438 *Experimental Astronomy* 40, 501-522.
- 1439 Turrini, D., Svetsov, V., Consolmagno, G., Sirono, S., Pirani, S. 2016. Olivine
1440 on Vesta as exogenous contaminants brought by impacts: Constraints from
1441 modeling Vesta's collisional history and from impact simulations. *Icarus*
1442 280, 328-339.
- 1443 Walsh, K. J., Morbidelli, A., Raymond, S. N., O'Brien, D. P., Mandell,

- 1444 A. M. 2011. A low mass for Mars from Jupiter's early gas-driven migration.
1445 Nature 475, 206-209.
- 1446 Wang, H., Weiss, B. P., Bai, X.-N., Downey, B. G., Wang, J., Wang, J.,
1447 Suavet, C., Fu, R. R., Zucolotto, M. E. 2017. Lifetime of the solar nebula
1448 constrained by meteorite paleomagnetism. Science 355, 623-627.
- 1449 Weidenschilling, S. J. 1975. Mass loss from the region of Mars and the asteroid
1450 belt. Icarus 26, 361-366.
- 1451 Weidenschilling, S. J. 1980. Dust to planetesimals - Settling and coagulation
1452 in the solar nebula. Icarus 44, 172-189.
- 1453 Weidenschilling, S. J., Davis, D. R., Marzari, F. 2001. Very early collisional
1454 evolution in the asteroid belt. Earth, Planets, and Space 53, 1093-1097.
- 1455 Weidenschilling, S. J. 2008. Accretion of planetary embryos in the inner and
1456 outer solar system. Physica Scripta Volume T 130, 014021.
- 1457 Weidenschilling, S. J. 2011. Initial sizes of planetesimals and accretion of the
1458 asteroids. Icarus 214, 671-684.
- 1459 Wetherill G. W., 1992. An alternative model for the formation of asteroids.
1460 Icarus 100, 307-325

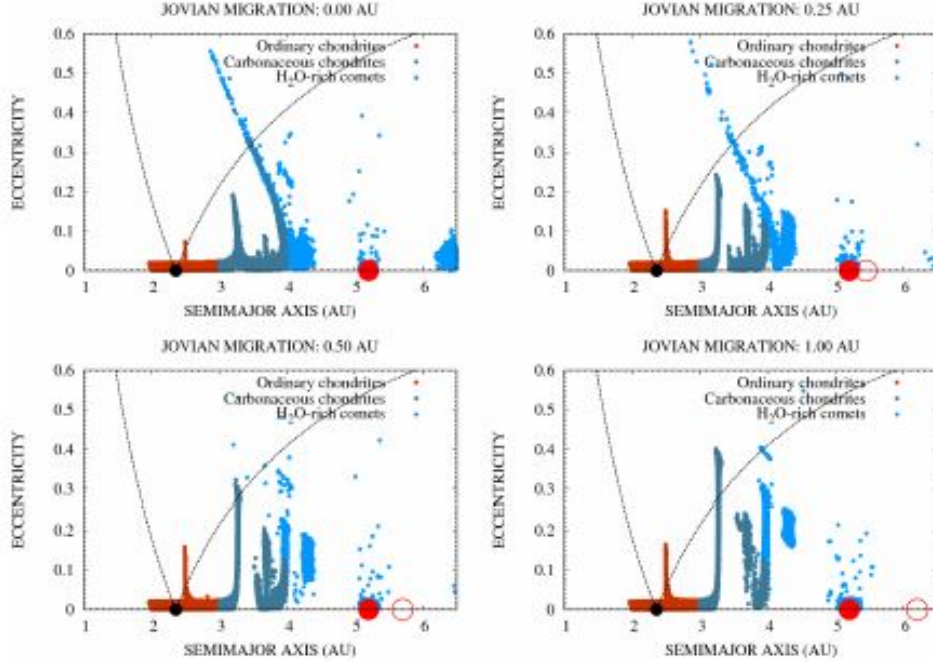


Figure 1: Dynamical excitation and radial mixing of the planetesimals in the circumstellar disc in response to Jupiter's mass growth and migration in the simulations by Turrini et al. (2011). The plots show snapshots of the Jovian Early Bombardment 0.2 Myr after the beginning of Jupiter's rapid gas accretion in the four migration scenarios considered by Turrini et al. (2011). The open red circles are the positions of Jupiter at the beginning of the simulations, the bigger red filled ones are the positions of Jupiter once fully formed (see Sect. 4.1). The smaller black filled circles at 2.36 au mark the orbital position of Vesta. The rocky asteroidal planetesimals analogous to ordinary chondrites that formed between 2 and 3 au are indicated in red (see Sect. 4.3). The rocky but water-enriched asteroidal planetesimals analogous to carbonaceous chondrites that formed between 3 and 4 au are indicated in dark cyan (see Sect. 4.3). The ice-rich cometary planetesimals that formed beyond 4 au are indicated in blue (see Sect. 4.3). Planetesimals inside the region delimited by the two black dotted curves are those that can impact Vesta.

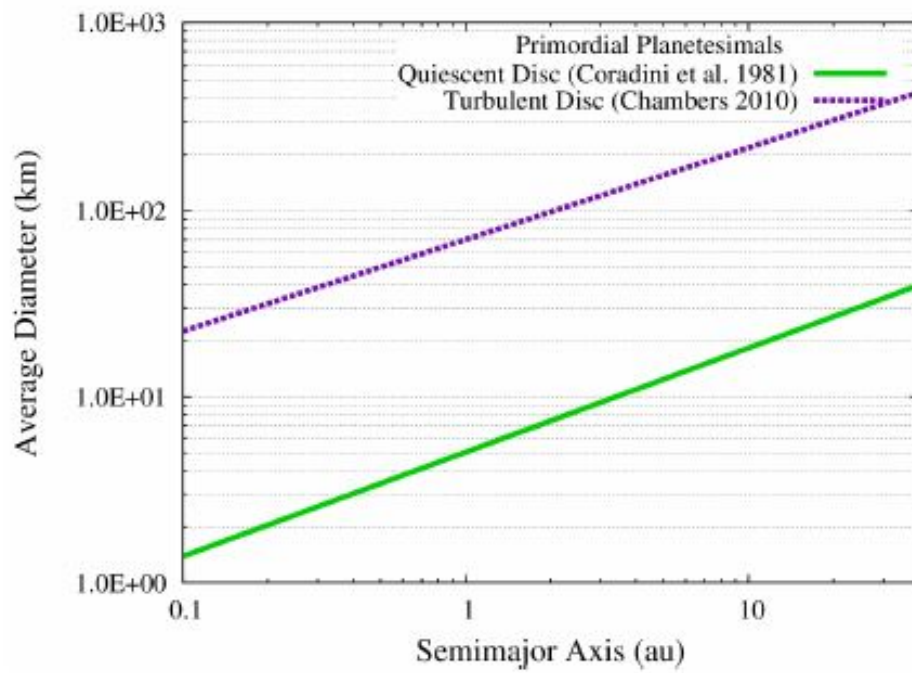


Figure 2: Comparison between the average diameters of the planetesimals as a function of their orbital distance from the Sun for the two primordial SFDs considered in our case study (see Sects. 4.3.1 and 4.3.2 for details).

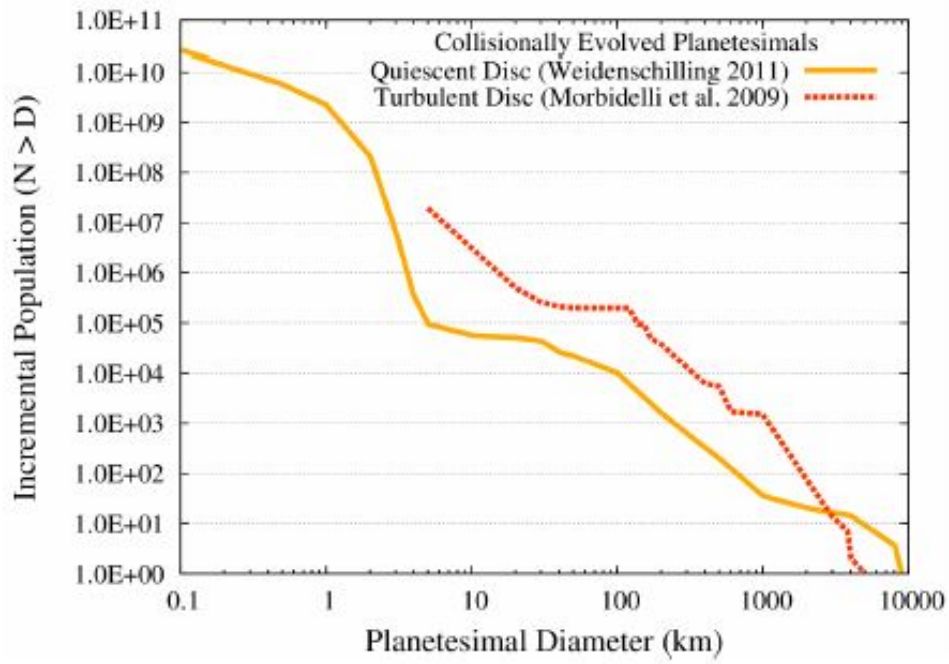


Figure 3: Comparison between the two collisionally-evolved SFDs considered in our case study in the orbital region comprised between 2 and 3 au (see Sects. 4.3.3 and 4.3.4 for details).

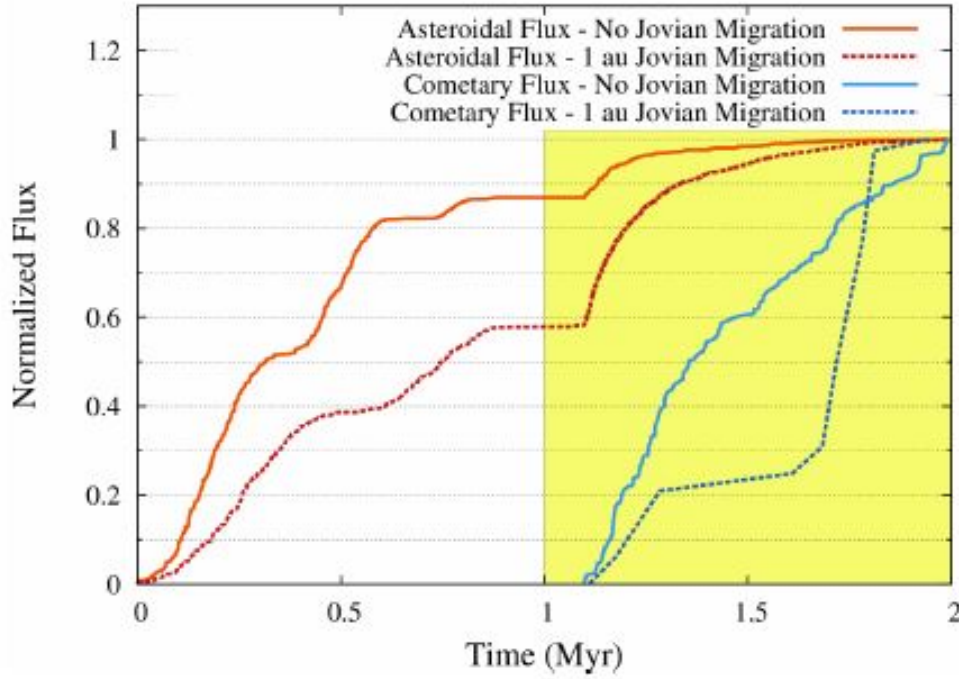


Figure 4: Normalized temporal distribution of the fluxes of asteroidal impactors (the orange and red lines) and cometary impactors (the light and dark blue lines) on Vesta in the no migration scenario (the solid lines) and the 1 au migration scenario (the dashed lines) for Jupiter. The highlighted area indicates the temporal interval over which we computed the late accretion and erosion of Vesta's crust, i.e. the Jovian Early Bombardment. Asteroidal impacts before this time were characterized by low velocities (< 1 km/s) and were not considered to account for the clearing effects of Vesta's formation on the orbital region surrounding the asteroid. As can be immediately seen, the Jovian migration enhances the flux of high-velocity (> 1 km/s) asteroidal impactors on Vesta while at the same time decreasing and making more erratic the flux of cometary impactors (see also Fig. 1).

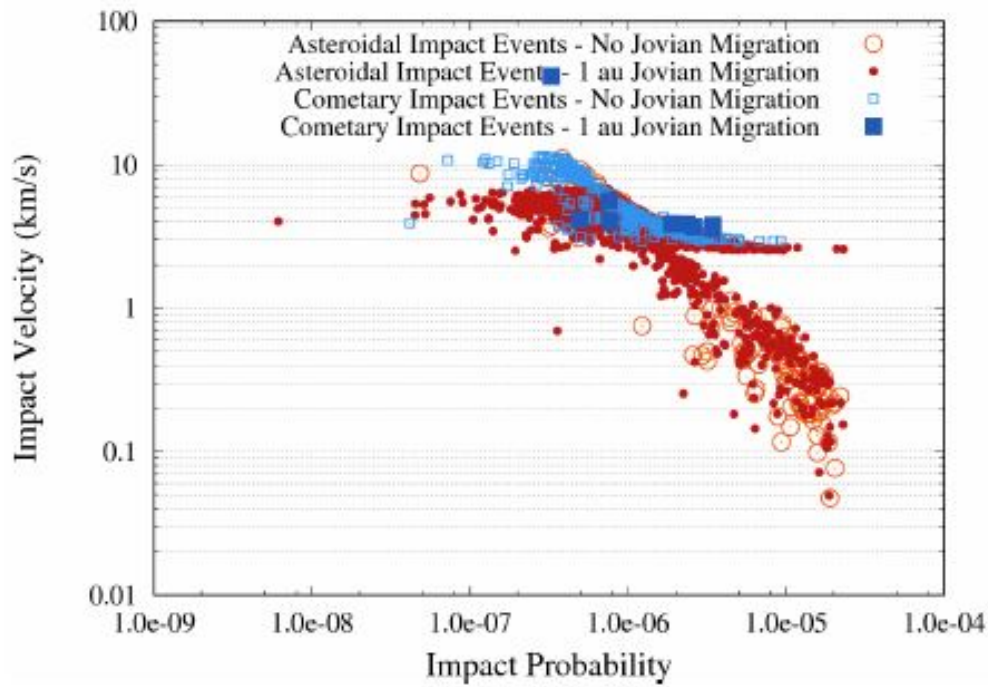


Figure 5: Distribution of the impact probabilities and impact velocities of the asteroidal and cometary impactors in the scenario of no migration of Jupiter and in the 1 au migration scenario for the giant planet in the simulations from Turrini et al. (2011). Note that the impact probabilities reported here refer to the individual impact events and are not impact probabilities averaged over the whole populations of impactors as in classical collisional algorithms (see e.g. O'Brien and Sykes 2011 and references therein).

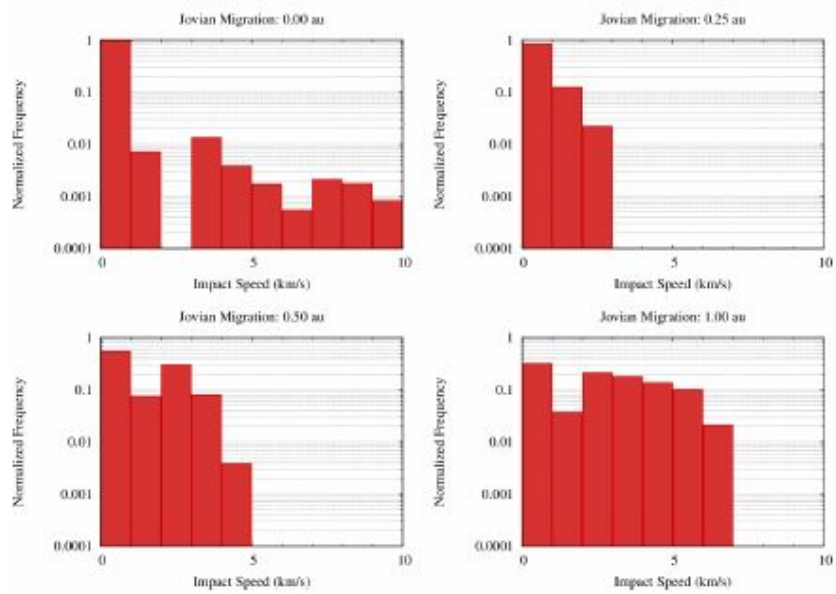


Figure 6: Normalized distribution of the impact velocities of the asteroidal impactors (i.e. the impactors originating between 1 and 4 au in the simulations of Turrini et al. 2011) on Vesta in the four migration scenarios considered in our case study (see Turrini et al. 2011 and Turrini 2014 for more details).

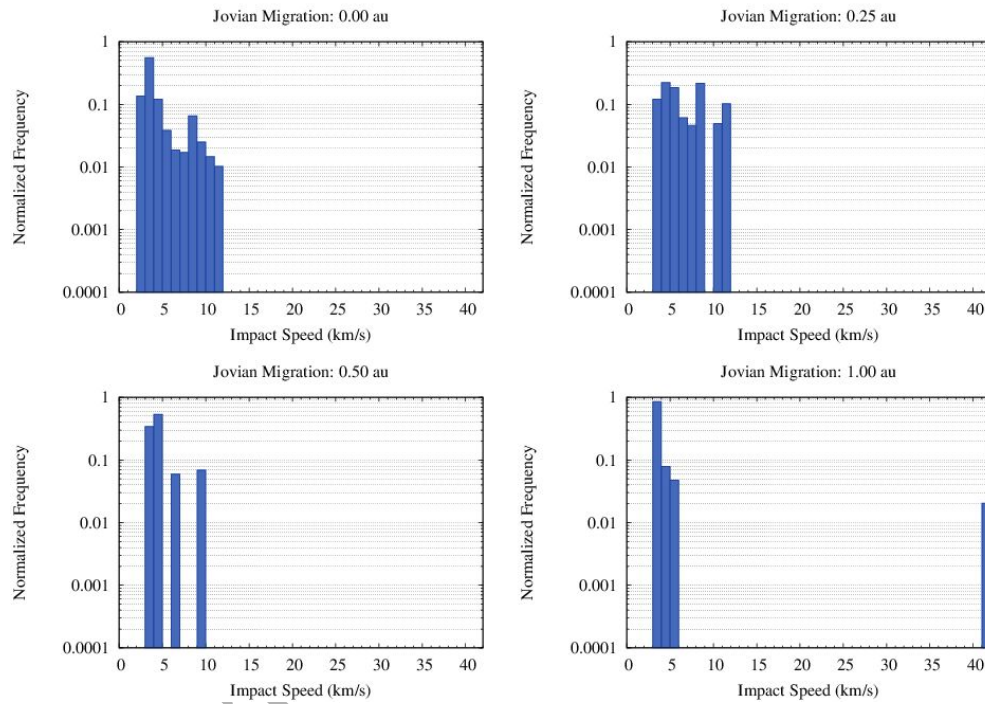


Figure 7: Normalized distribution of the impact velocities of the cometary impactors (i.e. the impactors originating between 4 and 10 au in the simulations of Turrini et al. 2011) on Vesta in the four migration scenarios considered in our case study (see Turrini et al. 2011 and Turrini & Svetsov 2014 for more details).

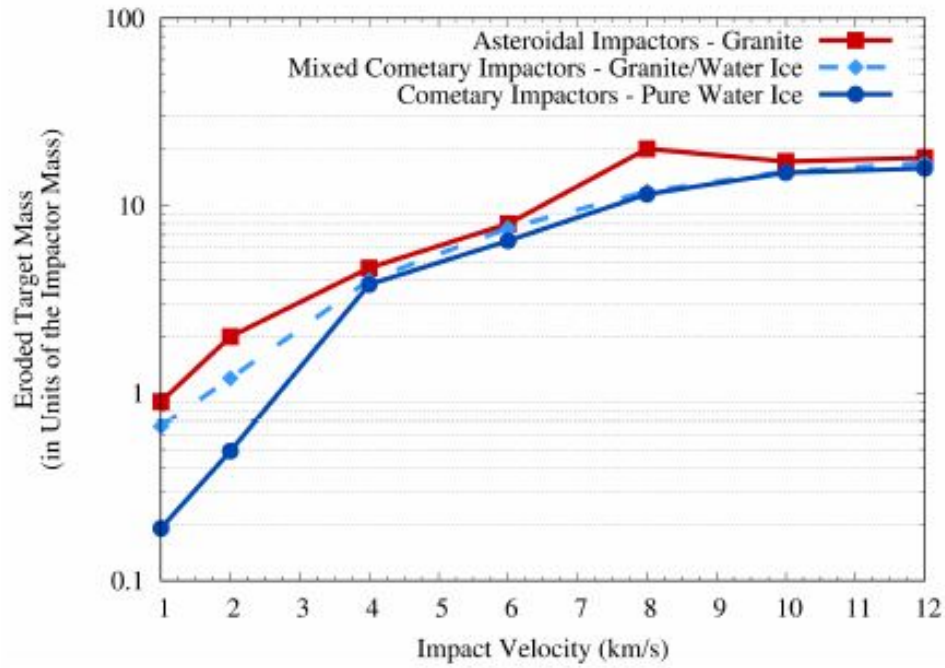


Figure 8: Fraction of the mass of the target body Vesta that is eroded and lost due to the impact, in units of the mass of the projectile. The different curves show the results from the simulations of Turrini et al. (2016) for asteroidal impactors made of granite (red solid line with filled squares), the simulations performed in this work for mixed granite-water ice cometary impactors (light blue dashed lines with filled diamonds), and, for comparisons, the results of the simulations of Turrini & Svetsov (2014) for cometary impactors made of pure water ice (blue solid line with filled circles).

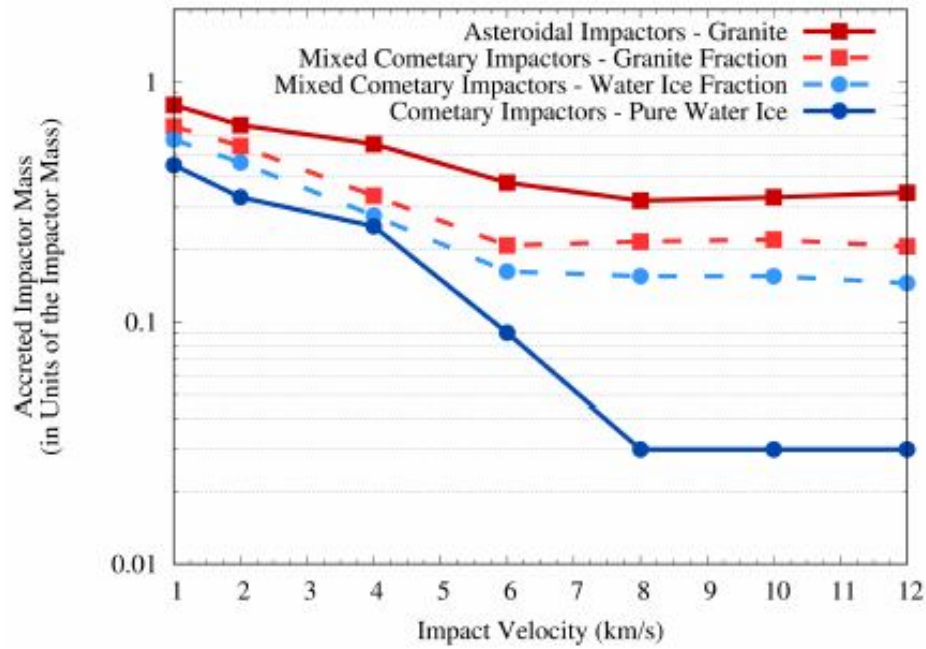


Figure 9: Fraction of the mass of the projectile that survives the impact and is accreted by Vesta, in units of the mass of the projectile. The different curves show the results from the simulations of Turrini et al. (2016) for asteroidal impactors made of granite (red solid line with filled squares), the simulations performed in this work for mixed granite-water ice cometary impactors (red dashed lines with filled squares for the rocky component and blue dashed lines with filled circles for the icy component), and, for comparisons, the results of the simulations of Turrini & Svetsov (2014) for cometary impactors made of pure water ice (blue solid line with filled circles).

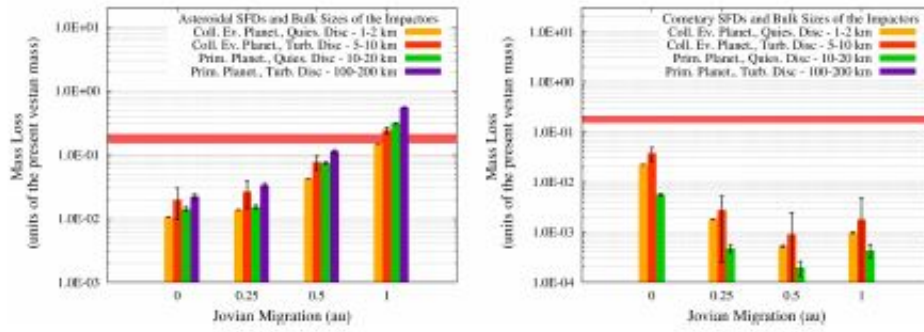


Figure 10: Mass loss experienced by a primordial Vesta with mass similar to that of the present Vesta due to (*left*) asteroidal impactors and (*right*) cometary impactors during Jupiter's mass growth in the different migration scenarios and for the different SFDs considered. For each SFD we report the characteristic diameter of the planetesimals producing the bulk of the impact flux as computed with our Monte Carlo methods. The horizontal regions highlighted in red mark the range of values of Vesta's crustal mass fraction and represent our upper boundary to Vesta's mass loss (see Sect. 3 and Consolmagno et al. 2015). Note that, given that the temporal interval considered in this proof-of-concept study is smaller than the timespan over which Vesta's crust can be eroded, only those scenarios producing mass losses *below* the red regions should be considered compatible with present-day Vesta.

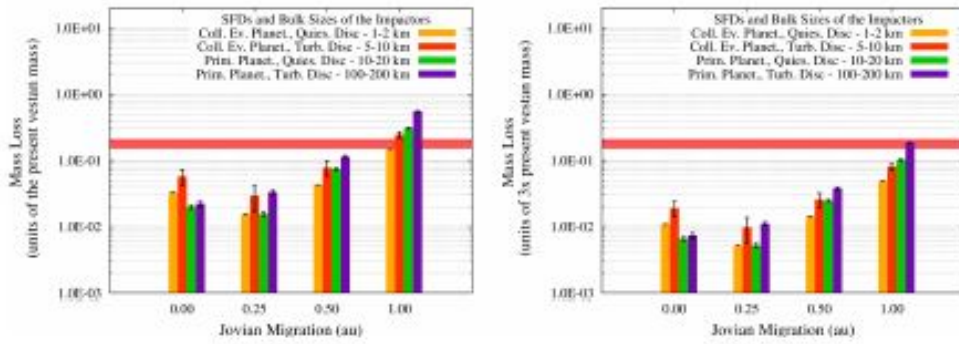


Figure 11: Total mass loss experienced by (*left*) a primordial Vesta with the same mass as present Vesta and (*right*) a primordial Vesta three times as massive during Jupiter's mass growth in the different migration scenarios and for the different SFDs considered. For each SFD we report the characteristic diameter of the planetesimals producing the bulk of the impact flux as computed with our Monte Carlo methods. The horizontal regions highlighted in red mark the range of values of Vesta's crustal mass fraction and represent our upper boundary to Vesta's mass loss (see Sect. 3 and Consolmagno et al. 2015). Note that, given that the temporal interval considered in this proof-of-concept study is smaller than the timespan over which Vesta's crust can be eroded, only those scenarios producing mass losses *below* the red regions should be considered compatible with present-day Vesta.

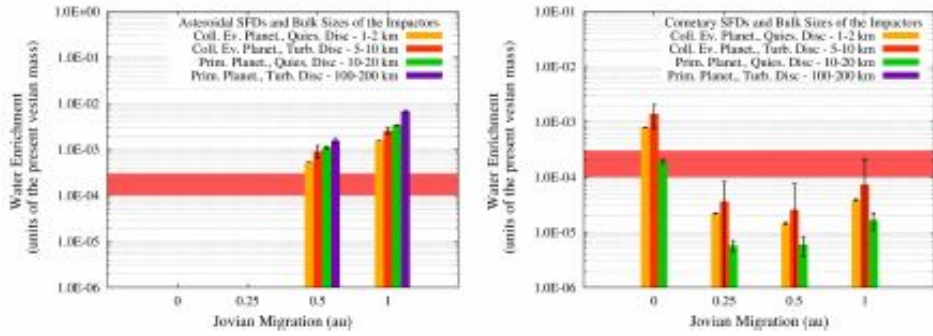


Figure 12: Water accretion experienced by a primordial Vesta with mass similar to that of the present Vesta due to (*left*) asteroidal impactors and (*right*) cometary impactors during Jupiter's mass growth in the different migration scenarios and for the different SFDs considered. For each SFD we report the characteristic diameter of the planetesimals producing the bulk of the impact flux as computed with our Monte Carlo methods. The horizontal regions highlighted in red mark the range of values of Vesta's water enrichment and represent our upper boundary to Vesta's water accretion (see Sect. 3 and [Stephant et al. 2016a,b](#); [Sarafian et al. 2017a,b](#)). Note that, given that the temporal interval considered in this proof-of-concept study is smaller than the timespan over which Vesta's crust can be enriched in water, only those scenarios producing water enrichments *below* the red regions should be considered compatible with present-day Vesta.

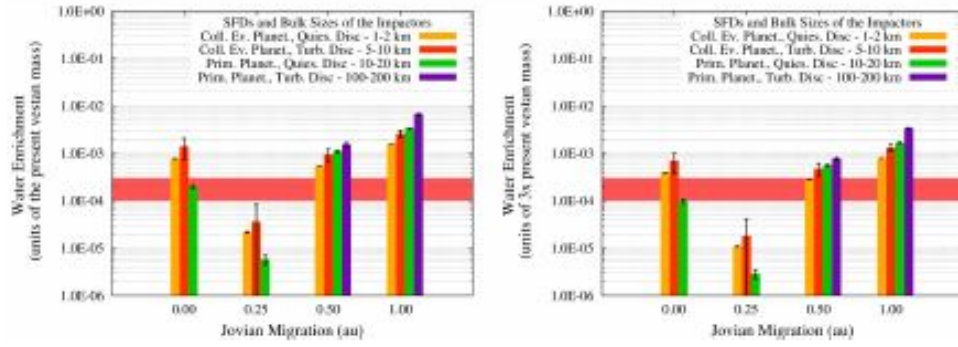


Figure 13: Total water accretion experienced by (*left*) a primordial Vesta with the same mass as the present Vesta and (*right*) a primordial Vesta three times as massive during Jupiter's mass growth in the different migration scenarios and for the different SFDs considered. For each SFD we report the characteristic diameter of the planetesimals producing the bulk of the impact flux as computed with our Monte Carlo methods. The horizontal regions highlighted in red mark the range of values of Vesta's water enrichment and represent our upper boundary to Vesta's water accretion (see Sect. 3 and [Stephant et al. 2016a,b](#); [Sarafian et al. 2017a,b](#)). Note that, given that the temporal interval considered in this proof-of-concept study is smaller than the timespan over which Vesta's crust can be enriched in water, only those scenarios producing water enrichments *below* the red regions should be considered compatible with present-day Vesta.

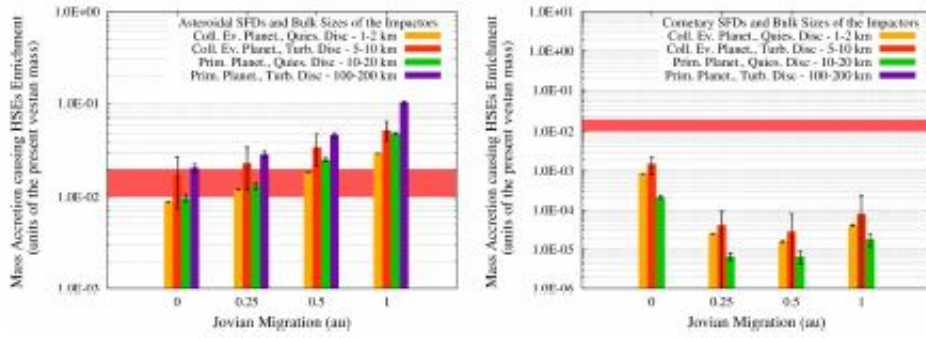


Figure 14: Mass accretion responsible for the HSEs enrichment experienced by a primordial Vesta with mass similar to that of the present Vesta due to (*left*) asteroidal impactors and (*right*) cometary impactors during Jupiter’s mass growth in the different migration scenarios and for the different SFDs considered. For each SFD we report the characteristic diameter of the planetesimals producing the bulk of the impact flux as computed with our Monte Carlo methods. The horizontal regions highlighted in red mark the range of values of Vesta’s mass accretion needed to produce the observed HSEs enrichment and represent our upper boundary to Vesta’s mass accretion (see Sect. 3 and Day et al. 2012). Note that, given that the temporal interval considered in this proof-of-concept study is smaller than the timespan over which Vesta’s crust can be enriched in HSEs, only those scenarios producing mass accretions *below* the red regions should be considered compatible with present-day Vesta.

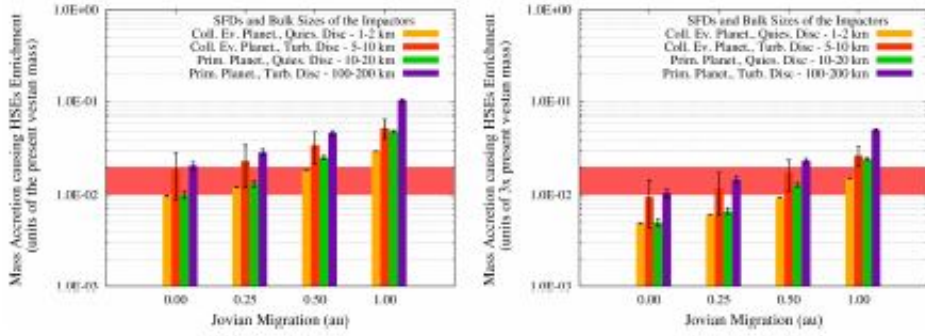


Figure 15: Total mass accretion responsible for the HSEs enrichment experienced by (*left*) a primordial Vesta with the same mass as present Vesta and (*right*) a primordial Vesta three times as massive during Jupiter’s mass growth in the different migration scenarios and for the different SFDs considered. For each SFD we report the characteristic diameter of the planetesimals producing the bulk of the impact flux as computed with our Monte Carlo methods. The horizontal regions highlighted in red mark the range of values of Vesta’s mass accretion needed to produce the observed HSEs enrichment and represent our upper boundary to Vesta’s mass accretion (see Sect. 3 and Day et al. 2012). Note that, given that the temporal interval considered in this proof-of-concept study is smaller than the timespan over which Vesta’s crust can be enriched in HSEs, only those scenarios producing mass accretions *below* the red regions should be considered compatible with present-day Vesta.